ENERGY-EFFICIENT COATINGS BASED ON WO_3-METAL MULTILAYERS

BY

Abdulaziz Hussain Alaswad

A Thesis Presented to the
DEANSHIP OF GRADUATE STUDIES

KING FAHD UNIVERSITY OF PETROLEUM & MINERALS
DHAHRAN, SAUDI ARABIA

In Partial Fulfillment of the
Requirements for the Degree of

MASTER OF SCIENCE

In

PHYSICS

January, 2009

KING FAHD UNIVERSITY OF PETROLEUM AND MINERALS

DHARAN 31261, SAUDI ARABIA

DEANSHIP OF GRADUATE STUDIES

This thesis, written by **ABDULAZIZ HUSSAIN ALASWAD** under the direction of his thesis advisor and approved by his thesis committee, has been presented to and accepted by the Dean of Graduate Studies, in partial fulfillment of the requirements for the degree of **MASTER OF SCIENCE IN PHYSICS**.

THESIS COMMITTEE

Dr. M. F. Al-Kuhaili (Advisor)

Prof. S. M. Ayub (Co-advisor)

Prof. N. Tabet (Member)

Prof. M. A. Gondal (Member)

Dr. A. Al-Shukri (Member)

Dr. Abdulaziz M. Aljalal
Department Chairman

Dr. Salam A. Zummo
Dean of Graduate Studies

12/4/09
Date

I would like to dedicate my thesis to

My parents

My wife

and My son Abdurrahman

Acknowledgements

My deep appreciation goes to my thesis advisor, Dr. Mohammad Al-Kuhaili, for his continuous help, guidance and the countless hours of attention he devoted during this work. I am also thankful and grateful to my thesis co-advisor Dr. Sardar Durrani for his great experimental experience that helped in the work. Thanks are also due to my thesis committee members (Dr. Ali Al-Shukri, Dr. Nouar Tabet and Dr. Mohammad Gondal) for their useful comments on the thesis. Heartfelt thanks are also due to Mr. Imran, who helped me a lot during the AFM and thickness measurements. Also, I would like to thank my colleagues who helped me through my study, especially my friends Abdullah Baziyad and Mahdi Al- Maghrabi.

Acknowledgment is due to King Fahd University of Petroleum and Minerals for supporting this research.

I wish to express my heartfelt gratitude to my parents for their encouragement, prayers and continuous support. Also, I would like to express my sincere appreciation to my dear wife for her great patience and motivation. I owe great thanks to my brothers and sisters for their encouragement.

Table of Contents

List of Figures

List of Tables

List of Symbols

B: Magnetic field

c: Speed of light

d: Thickness of the film

e: Electron's charge

E: Electric field

E_g: Energy gap

f: Frequency

F: Figure of merit ($T_{VIS} \times R_{IR}$)

k: Extinction coefficient

m_e: Electron's mass

$\hat{n}$: Index of refraction

n: Refractive index

N_f: Number of free electron

P: Polarization

R: Reflectance

R_{IR}: Average infrared reflectance

t: Time

T: Transmittance

T_{VIS}: Average visible transmittance

v: velocity

Φ: Penetration depth

ρ: Reflectance coefficient

τ: Transmittance coefficient

δ: Phase difference

λ: Wavelength

ω: Angular frequency

THESIS ABSTRACT

NAME OF STUDENT : ABDULAZIZ HUSSAIN ALASWAD

TITLE OF STUDY : ENERGY EFFICIENT COATINGS BASED ON WO_3-METAL MULTILAYERS

MAJOR FIELD : Physics

DATE OF DEGREE : January, 2009

Transparent heat mirrors based on WO_3-metal multilayers on fused silica substrate were fabricated by using thermal evaporation. The metals were silver and gold. The fabricated multilayers had two and three layers as follows: (WO_3/Ag), (WO_3/Au), (WO_3/Ag/WO_3), and (WO_3/Au/WO_3). The optical and morphological properties of single layers of Ag, Au and WO_3 were investigated to serve as a preliminary guide to the fabrication of transparent heat mirrors. The optical properties (reflectance and transmittance) of the multilayers were measured over the visible and near infrared regions, and their dependence on the thickness of the metal layer was investigated. The optimum conditions producing high visible transmittance and high infrared reflectance were determined. It was found that three layers are better than two layers and the coating (WO_3/Ag/WO_3) showed the best quality of transparent heat mirrors.

ملخص الرسالة

الاسم: عبدالعزيز بن حسين بن محمد الأسود

عنوان الرسالة: الطبقات الشفافة العازلة للحرارة المكونة من رقائق متعددة الطبقات من أكسيد التنغستن وعنصر الفضة أو الذهب.

تاريخ منح الدرجة: محرم 1430هـ (يناير 2009م)

تمت عملية تحضير الطبقات الشفافة العازلة للحرارة متعددة الطبقات بواسطة التبخير الحراري. كان عدد الطبقات في الطلاءات المحضرة إما طبقتين أو ثلاث طبقات على النحو التالي: (WO_3/Ag) و (WO_3/Au) و $(WO_3/Ag/WO_3)$ و $(WO_3/Au/WO_3)$. بدأنا بدراسة الخواص الضوئية و تضاريس السطوح لطبقات وحيدة من الفضة و الذهب و أكسيد التنغستن والتي ساعدت في الوصول الى تحضير الطلاءات العازلة للحرارة. كما تم قياس النفاذية والإنعكاسية للأشعة المرئية وتحت الحمراء ومعرفة مدى اعتمادها على سمك المعدن (الذهب أو الفضة) في الطبقات. وأخيرا تم تحديد السمك الأمثل لكل طبقة و الذي ينتج أفضل عوازل ممكنة والتي تتميز بالشفافية العالية والعزل للحرارة في نفس الوقت، كما وجد أن الثلاث طبقات أفضل من الطبقتين في انتاج مثل هذه العوازل الحرارية.

Chapter 1: INTRODUCTION

1.1 Optical Properties of Metals

A great deal of our knowledge of the optical properties of solids has been elucidated by studying the interaction of light with the valence electrons of these materials. In this section, the optical constants, which are the index of refraction ($\tilde{n}$), extinction coefficient (k) and reflectance (R), will be discussed and defined for metals. The information presented below follows closely that of reference [1].

1.1.1 Index of refraction

It is a well-known phenomenon that light changes its path or refracts as it passes from a less dense medium to an optically denser medium, as shown in Figure 1.1. The angle of refraction β is smaller than the angle of incidence α. If the first medium is vacuum and the second is any other medium, the refractive index n of the medium can be defined as:

$$n = \frac{n_{med}}{n_{vac}} = \frac{\sin(\alpha)}{\sin(\beta)} \tag{1.1}$$

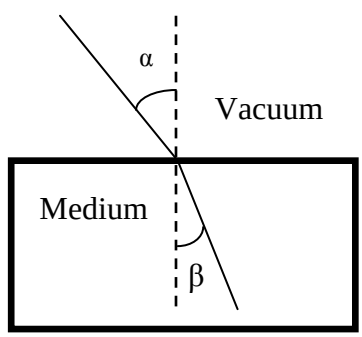

Figure 1.1: Refraction of light as it passes from vacuum to a dense medium.

where n_{vac} is set to be unity. The refractive index of air is approximately the same as that of a vacuum. The different velocities of light in the two media cause the refraction of light. The velocity of light in any medium is given by:

$$v = \frac{\sin(\beta)}{\sin(\alpha)} c \tag{1.2}$$

where c is the velocity of light in a vacuum. Thus, the refractive index can be defined as:

$$n = \frac{c}{v} \tag{1.3}$$

The value of n changes according to the wavelength of the incident light. This phenomenon is called dispersion.

1.1.2 Extinction coefficient (k)

The index of refraction is a complex quantity, and it can be written as $\hat{n} = n - ik$. The real part n is the refractive index, while the imaginary part k is called the extinction coefficient or damping constant. To understand why k is termed the damping constant, consider a plane polarized wave propagating along the z-axis and vibrating in the x-direction as shown in Figure 1.2.

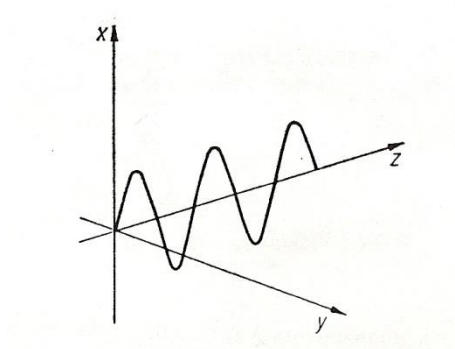

Figure 1.2: Plane polarized wave which propagates in the positive *z*-direction and vibrates in the *x*-direction [1].

Consider a medium having its surface in the *xy*-plane and its bulk along the *z*-direction. When the plane polarized wave passes through the medium, the complete solution of the electric field in the medium is:

$$E_x = E_0 \exp\left[-\frac{\omega k}{c} z\right] \exp\left[\mathrm{i}\omega\left(\mathrm{t} - \frac{\mathrm{zn}}{\mathrm{c}}\right)\right] \tag{1.4}$$

where E_0 is the maximum amplitude of the electric field, ω = 2πf is the angular frequency of the wave, and *t* is the time. The first term $E_0 \exp\left[-\frac{\omega k}{c} z\right]$ is the damping amplitude which is responsible for decreasing the wave exponentially with increasing *z*, as shown in Figure 1.3. The second term is an undamped sinusoidal wave. The value of *k* determines the degree of damping of the light wave. That is, when the value of *k* is large, the wave decays fast.

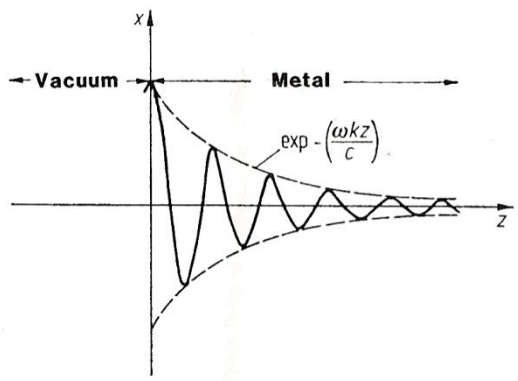

Figure 1.3: Exponential decay of the electric field as it passes through a metal. [1]

Generally, metals have an extinction coefficient k that is large compared to other materials. Thus, metals damp the intensity of light in a relatively short distance. Practically, measuring the field strength E in Eq.1.4 is very difficult. Therefore, the intensity of light, which is equal to the modulus square of E, is commonly measured. The intensity I can be measured easily by using sensitive devices, such as photomultiplier tubes. The intensity can be calculated from Eq.1.4:

$$I(z) = |E|^2 = I_0 \exp\left(-\frac{2\omega k}{c} z\right) \tag{1.5}$$

where $I_o = |E_o|^2$. Now, let us define a characteristic penetration depth Φ which measures how deeply light can penetrate into the material. Φ is defined as the depth at which the intensity of the light inside the material I(z) falls to 1/e of its original value at the surface I_0, namely when:

$$I(z) = \frac{1}{e} I_0 \tag{1.6}$$

Using Equations 1.5 and 1.6, the penetration depth Φ may be written as:

$$\Phi = \frac{c}{2\omega k} = \frac{c}{4\pi f k} = \frac{\lambda}{4\pi k} \tag{1.7}$$

Therefore, when k is large, as in metals, the penetration depth is small, and vice versa. Table 1.1 gives values of k and Φ for different materials when the incident light is sodium lamp light (λ =589.3 nm).

Table 1.1: Values of the damping constant k and penetration depth Φ for different materials [1].

Material	Water	Flint glass	Graphite	Gold	Silver
Φ (cm)	32	29	6×10^{-6}	1.5×10^{-6}	1.2×10^{-6}
k	1.4×10^{-7}	1.5×10^{-7}	0.8	3.2	4.0

1.1.3 Reflectance (R)

It is well-known that metals have a large reflectance to light. This is because light penetrates only a short distance in a metal as shown in Figure 1.3. Therefore, a small amount of the incident energy is converted into heat, while the major part of the energy is reflected. Table 1.2 shows the reflectance of some metals at a wavelength of 600 nm.

Table 1.2: Optical constants and reflectance R of some metals at λ=600 nm. [1]

Metal	n	k	R[%]
Copper	0.14	3.35	95.6
Silver	0.05	4.09	98.9
Gold	0.21	3.24	92.9
Aluminum	0.97	6.00	90.3

The reflectance can be defined as the ratio between the reflected intensity I_R and the incident intensity I_0:

$$R = \frac{I_R}{I_0} \tag{1.8}$$

The reflectance of light, that is normally incident on a material, is given by:

$$R = \left|\frac{\hat{n} - 1}{\hat{n} + 1}\right|^2 \tag{1.9}$$

which yields *Beer's equation*:

$$R = \frac{n - ik - 1}{n - ik + 1} \cdot \frac{n + ik - 1}{n + ik + 1} = \frac{(n-1)^2 + k^2}{(n+1)^2 + k^2} \tag{1.10}$$

Reflectance is a function of the wavelength of light, since n depends on wavelength. Also, the reflectance can be written as a function of the dielectric function $\hat{\varepsilon}$. The dielectric function is generally a complex quantity given by ($\hat{\varepsilon} = \varepsilon - i\frac{2\sigma}{f}$) where ε is the dielectric constant, σ is the (a.c.) conductivity and f is the light frequency. $\hat{\varepsilon}$ relates to the index of refraction ($\hat{n} = n - ik$) by the equation:

$$\hat{n}^2 = \hat{\varepsilon} \tag{1.11}$$

Then $(n^2 - k^2) - i\,2nk = \varepsilon - i\frac{2\sigma}{f}$ (1.12)

Equating the real parts yields

$$\varepsilon = \varepsilon_1 = n^2 - k^2 \tag{1.13}$$

and equating the imaginary parts yields

$$\frac{2\sigma}{f} = \varepsilon_2 = 2nk \tag{1.14}$$

The notations ε_1 and ε_2 are introduced for simplicity.

Using Eq. 1.13 and 1.14 and after some transformation, Eq. 1.10 is rewritten as

$$R = \frac{\sqrt{\varepsilon_1^2 + \varepsilon_2^2} + 1 - \sqrt{2(\sqrt{\varepsilon_1^2 + \varepsilon_2^2} + \varepsilon_1)}}{\sqrt{\varepsilon_1^2 + \varepsilon_2^2} + 1 + \sqrt{2(\sqrt{\varepsilon_1^2 + \varepsilon_2^2} + \varepsilon_1)}} \tag{1.15}$$

Hagen and Rubens did an approximation to Eq. 1.15 to derive the following relationship between the reflectance and conductivity of metals for small frequencies (far infrared) where ($f/\sigma \ll 1$ or $\varepsilon_2 \gg \varepsilon_1$):

$$R = 1 - 2\sqrt{\frac{f}{\sigma}} \tag{1.16}$$

This is called the Hagen-Rubens equation, which states that metals with large electrical conductivity are good reflectors in the infrared (IR) region.

1.1.4 Plasma frequency

In the near IR and visible region, the Hagen-Rubens equation is no longer valid. Thus, the atomic structure needs to be considered by using the Drude model. Drude postulated that some electrons in a metal can be considered to be free and also can be

accelerated by an external electric field. Now, consider the case where free electrons are excited under the influence of a plane polarized light wave of strength:

$$E = E_0 \exp(i\omega t) \tag{1.17}$$

The equation describing the motion of electrons can be written by using Newton's second law:

$$F = ma \tag{1.18}$$

$$eE = m_e \frac{d^2x}{dt^2} \tag{1.19}$$

where e and m_e are the charge and mass of an electron, respectively. The stationary solution of this differential equation is obtained by substituting the second derivative of a trial solution $x = x_0 \exp(i\omega t)$ into Eq. 1.19 and this produces

$$x = -\frac{eE}{4\pi^2 m_e f^2} \tag{1.20}$$

The polarization P, which is defined as the sum of the dipole moments of all free electrons (N_f), is given by

$$P = exN_f \tag{1.21}$$

The dielectric function $\hat{\varepsilon}$ is related to the polarization by:

$$\hat{\varepsilon} = 1 + 4\pi \frac{P}{E} \tag{1.22}$$

Inserting Eq. 1.20 and Eq. 1.21 into Eq. 1.22 yields

$$\hat{\varepsilon} = 1 - \frac{e^2 N_f}{\pi m_e f^2} \tag{1.23}$$

Substituting Eq. 1.11 into Eq. 1.23 yields

$$\hat{n}^2 = 1 - \frac{e^2 N_f}{\pi m_e f^2} \tag{1.24}$$

Now, consider two special cases:

1. For low frequencies, the term $\frac{e^2 N_f}{\pi m_e f^2}$ is greater than one, then $\hat{n}^2$ is negative and therefore $\hat{n} = ik$ where the real part n is zero. Substituting $n = 0$ in Eq. 1.10, the reflectance becomes 100%.

2. For high frequencies, the term $\frac{e^2 N_f}{\pi m_e f^2}$ is less than one, then $\hat{n}^2$ is positive and therefore $\hat{n} = n$ but smaller than one. Using Eq. 1.10, the reflectance becomes minimum and the material behaves like a transparent insulator.

The plasma frequency is defined as the frequency that separates the reflective region from the transparent region. This frequency can be obtained by setting $\frac{e^2 N_f}{\pi m_e f^2}$ equal to unity, which gives:

$$f = \sqrt{\frac{e^2 N_f}{\pi m_e}} \tag{1.25}$$

Therefore, the position of the plasma frequency is altered only by changing the free electrons concentration of the material.

1.2 Optical Properties of Semiconductors

The concept of the index of refraction and the extinction coefficient of semiconductors is the same as that of metal presented in section 1.1. In this section, the emphasis will be on the processes of absorption and emission of photons in semiconductors. In general, there are several mechanisms which can lead to the

absorption and emission processes. These mechanisms include: band-to-band, impurity-to-band, free-carrier, phonon and excitonic transitions. The focus here will be on the first mechanism, band-to-band transitions. [2]

In semiconductors, electrons are confined to the valence and conduction bands, while they are forbidden from other regions. The energy difference between the top of the valence band and the bottom of the conduction band is called the energy gap E_g. Electrons require a specific amount of energy to make a transition from one band to another. This energy can be provided by a photon if its energy $h\nu$ is greater than the energy gap E_g. The absorption process occurs when a photon with an appropriate energy ($h\nu \geq E_g$) is absorbed, resulting in an upward transition of the electron from the valence band to the conduction band, leaving a hole in the valence band. Thus, an electron-hole pair is created. This increases the concentration of mobile charge carriers, and therefore the conductivity of the material is enhanced. The emission process can occur in two ways: spontaneous and stimulated emission. In the spontaneous emission, the electron deexcites from the conduction to the valence band (electron-hole recombination) and emits a photon of energy $h\nu = E_g$. Light-emitting diodes (LEDs) operate on this basis. However, in the stimulated emission, the electron-hole recombination is stimulated by a photon. The result is the induced emission of an identical photon, and this process is responsible for the operation of lasers. Figure 1.4 shows the band-to-band absorption and emission processes. [2]

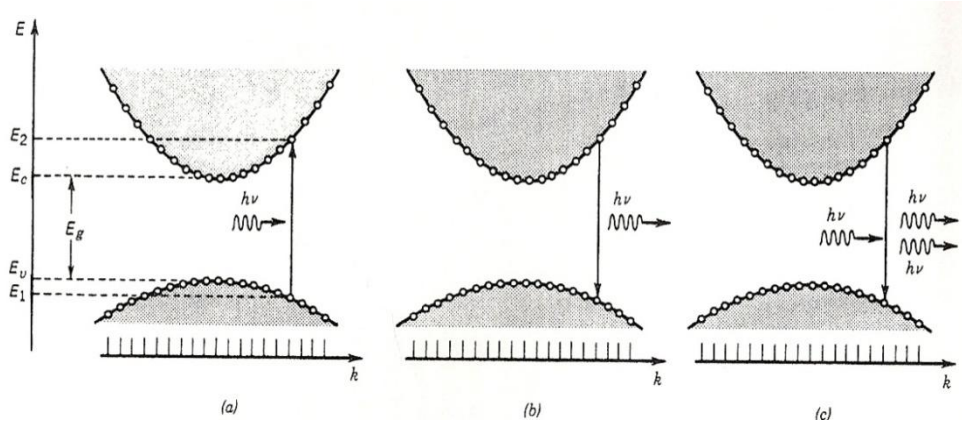

Figure 1.4: Absorption and emission processes in the band-to-band transition. (a) absorption of a photon, (b) spontaneous emission of a photon and (c) stimulated emission of a photon. [2]

1.3 Theory of Multilayer Coatings.

Multilayer coatings provide many useful and interesting applications of thin films, such as antireflection coatings, broad and narrow-band pass filters, smart windows, and heat mirrors. The theory of multilayer coating was presented in ref.[3], and is outlined below.

The equations required from electromagnetic theory are summarized here. The energy of an EM wave propagating in the direction of the Poynting vector is given by the relation:

$$\vec{\mathbf{S}} = \varepsilon_o c^2 \vec{\mathbf{E}} \times \vec{\mathbf{B}} \tag{1.26}$$

The relation between the magnitudes of electric and magnetic fields is given by:

$$E = \upsilon B \tag{1.27}$$

where υ is the wave speed, which depends on the refractive index (n) of the medium,

$$\upsilon = \frac{c}{n} \tag{1.28}$$

and the speed of light c equals

$$c = \frac{1}{\sqrt{\varepsilon_o \mu_o}} \tag{1.29}$$

where ε_o and μ_o are the permittivity and permeability of free space, respectively. Using the above equations, the magnitudes of magnetic and electric fields can be related by

$$B = \frac{E}{\upsilon} = \frac{E}{c / n} = n\sqrt{\varepsilon_o \mu_o}\, E \tag{1.30}$$

1.3.1 Transfer matrix

The transfer matrix is developed to optically represent a thin film and characterize its performance. It is used to calculate the reflectance and transmittance of multilayer films. In this approach, a non-absorbing film is treated. Consider Figure 1.5, shown below, where a beam of light is incident on a thin film of refractive index n and thickness d. The film is deposited on a substrate of refractive index n_s. The electric field of light is assumed to be polarized perpendicular to the plane of incidence. The air-film interface and the film-substrate interface are represented by (a) and (b) respectively. E_{r1} is the sum of all the multiply-reflected beams at interface (a), and E_{i2} is the sum of all the multiple beams at interface (b) and directed toward the substrate, and so on. In this way, we account for multiple beams in the interfaces.

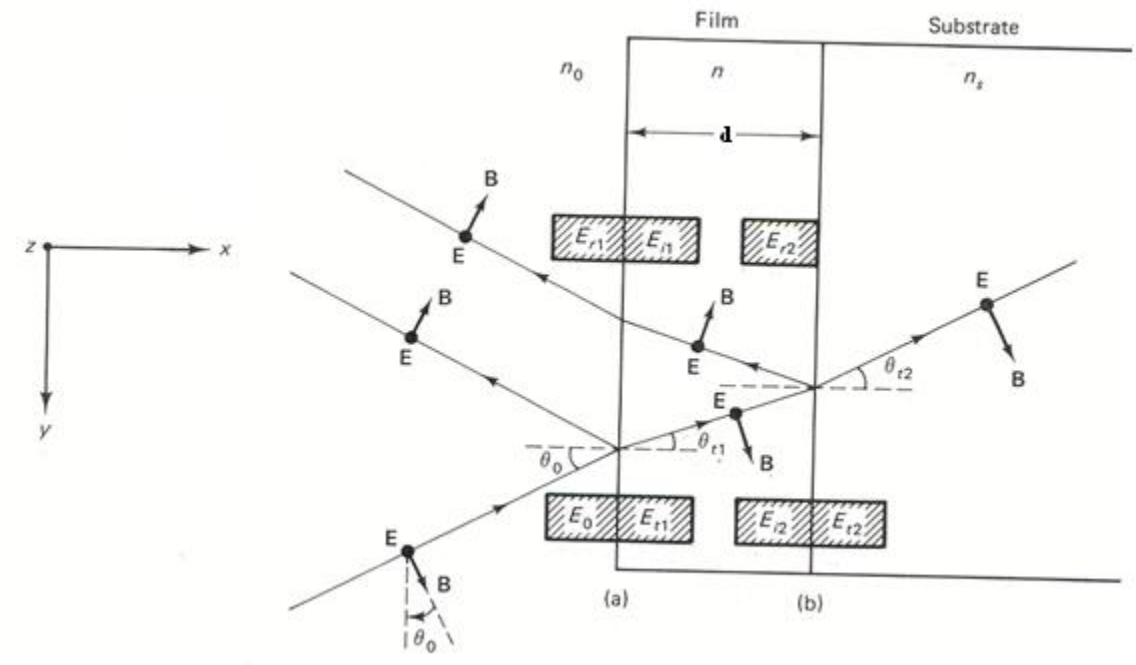

Figure 1.5: Reflection of a beam from a single layer with thickness *d*. The air-film interface and the film-substrate interface are represented by (a) and (b), respectively. [3]

The boundary conditions on the electric and magnetic fields require that their tangential components be continuous across each interface. In our case, *E* is always perpendicular to the plane of incidence. Therefore, the electric field is everywhere tangential to the planes at (a) and (b), whereas the magnetic field consists of both a tangential *y*-component and a perpendicular x-component. Therefore,

$$E_a = E_o + E_{r1} = E_{t1} + E_{i1} \tag{1.31}$$

$$E_b = E_{i2} + E_{r2} = E_{t2} \tag{1.32}$$

$$B_a = B_o \cos\theta_o - B_{r1}\cos\theta_o = B_{t1}\cos\theta_{t1} - B_{i1}\cos\theta_{t1} \tag{1.33}$$

$$B_b = B_{i2}\cos\theta_{t1} - B_{r2}\cos\theta_{t1} = B_{i2}\cos\theta_{t2} \tag{1.34}$$

Using $B = n\sqrt{\varepsilon_o \mu_o}\, E$, equations 1.33 and 1.34 become

$$B_a = \gamma_o (E_o - E_{r1}) = \gamma_1 (E_{t1} - E_{i1}) \tag{1.35}$$

$$B_b = \gamma_1 (E_{i2} - E_{r2}) = \gamma_2 E_{t2} \tag{1.36}$$

where

$$\gamma_o = n_o \sqrt{\varepsilon_o \mu_o} \cos\theta_o \tag{1.37}$$

$$\gamma_1 = n \sqrt{\varepsilon_o \mu_o} \cos\theta_{t1} \tag{1.38}$$

$$\gamma_s = n_s \sqrt{\varepsilon_o \mu_o} \cos\theta_{t2} \tag{1.39}$$

Note that E_{i2} differs from E_{t1} only because of a phase shift δ that develops due to one traversal of the film:

$$\delta = k_o \Delta = (\frac{2\pi}{\lambda_o}) nd \cos\theta_{t1} \tag{1.40}$$

Thus $E_{i2} = E_{t1}\, e^{-i\delta}$ and likewise $E_{i1} = E_{r2}\, e^{-i\delta}$.

Using matrices, the fields at interfaces (a) and (b) can be related as:

$$\begin{bmatrix} E_a \\ B_a \end{bmatrix} = \begin{bmatrix} \cos\delta & (i \sin\delta)/\gamma_1 \\ i\gamma_1 \sin\delta & \cos\delta \end{bmatrix} \begin{bmatrix} E_b \\ B_b \end{bmatrix} \tag{1.41}$$

The 2×2 matrix is called the transfer matrix of the film and it is represented generally by

$$\mathbf{M} = \begin{bmatrix} m_{11} & m_{12} \\ m_{21} & m_{22} \end{bmatrix} \tag{1.42}$$

In the case of N layers, each layer is represented by a transfer matrix, and the fields at the outer interfaces of the multilayer can be related by using a general matrix relation:

$$\begin{bmatrix} E_a \\ B_a \end{bmatrix} = \mathbf{M_1 M_2 M_3 \ldots M_N} \begin{bmatrix} E_N \\ B_N \end{bmatrix} \tag{1.43}$$

where E_N and B_N are the fields at the interface between the nth layer and the substrate.

The product of transfer matrices is given by

$$\mathbf{M_1 M_2 M_3 ... M_N} = \begin{bmatrix} m_{11} & m_{12} \\ m_{21} & m_{22} \end{bmatrix} \tag{1.44}$$

and by using the equations

$$\begin{bmatrix} E_o + E_{r1} \\ \gamma_o (E_o - E_{r1}) \end{bmatrix} \equiv \begin{bmatrix} m_{11} & m_{12} \\ m_{21} & m_{22} \end{bmatrix} \begin{bmatrix} E_{t2} \\ \gamma_2 E_{t2} \end{bmatrix} \tag{1.45}$$

Dividing the two equations by E_0 yields:

$$1 + \rho = m_{11}\,\tau + m_{12}\,\gamma_s\,\tau \tag{1.46}$$

$$\gamma_o\,(1 - \rho) = m_{21}\,\tau + m_{22}\,\gamma_s\,\tau \tag{1.47}$$

where ρ and τ are the reflectance and transmittance coefficients, respectively, given by:

$$\rho = E_{r1}/E_o \tag{1.48}$$

$$\tau = E_{t2}/E_o \tag{1.49}$$

Solving Eq. 1.46 and Eq. 1.47 gives:

$$\tau = \frac{2\gamma_o}{\gamma_o m_{11} + \gamma_o \gamma_s m_{12} + m_{21} + \gamma_s m_{22}} \tag{1.50}$$

$$\rho = \frac{\gamma_o m_{11} + \gamma_o \gamma_s m_{12} - m_{21} - \gamma_s m_{22}}{\gamma_o m_{11} + \gamma_o \gamma_s m_{12} + m_{21} + \gamma_s m_{22}} \tag{1.51}$$

Now, the transmittance ($T = \tau\,\tau^*$) and the reflectance ($R = \rho\,\rho^*$) can be calculated.

$$R = |\rho|^2 = \rho\rho^* = \frac{n^2 (n_o - n_s)^2 \cos^2\delta + (n_o n_s - n^2)^2 \sin^2\delta}{n^2 (n_o + n_s)^2 \cos^2\delta + (n_o n_s + n^2)^2 \sin^2\delta} \tag{1.52}$$

$$T = |\tau|^2 = \tau\tau^* = \frac{4n_o^2 \varepsilon_o \mu_o \cos^2\theta_o}{n^2(n_o + n_s)^2 \cos^2\delta + (n_o n_s + n^2)^2 \sin^2\delta} \tag{1.53}$$

1.3.2 Reflectance at normal-incidence

In the case of one layer at normal-incidence where $\theta_i = \theta_t = 0$, the elements of the transfer matrix become:

$m_{11} = \cos\delta$ $\qquad$ $m_{12} = (i\ c\ sin\ \delta)/n$

$m_{21} = (i\ n\ sin\ d)/c$ $\qquad$ $m_{22} = \cos\delta$

Taking the thickness of the film to be quarter-wavelength, $d = \lambda/4 = \lambda_o/(4\ n)$.

The phase difference is $\delta = (2\pi/\lambda_o)\ n\ d = (2\ \pi/\lambda_o)\ n\ (\lambda_o/4\ n) = \pi/2$, and $\cos\delta = 0$, $sin\ \delta = 1$.

Thus, the reflectance Eq.(1.52) is reduced to

$$R = \left(\frac{n_o n_s - n^2}{n_o n_s + n^2}\right)^2 \tag{1.54}$$

Therefore, a perfectly anti-reflecting ($R = 0$) film can in principle be fabricated with a coating of $\lambda/4$ thickness and a refractive index of $n = (n_o\ n_s)^{1/2}$. For a glass substrate (n_s=1.52), the refractive index of the films n should be 1.23. A dielectric with such a refractive index is not available. Therefore, a single film with zero reflectance cannot be fabricated. Equation (1.45) can be used to calculate the reflectance of a glass substrate by setting $n = n_o$. This gives a value of 4.3 %. However, if the substrate is coated with a $\lambda/4$ film of MgF_2 ($n = 1.38$), then R = 1.3 %.

1.3.3 Two-layer anti-reflecting films

Using a double layer of quarter-wave-thickness films of refractive indices n_1 and n_2, it is possible to achieve essentially zero reflectance at a specific wavelength with available coating materials. At normal-incidence, the transfer matrix of a single of quarter-wave thickness is:

$$\mathbf{M}_1 = \begin{bmatrix} 0 & i/\gamma_1 \\ i\gamma_1 & 0 \end{bmatrix} \tag{1.55}$$

The transfer matrix for two such layers is:

$$\mathbf{M} = \mathbf{M}_1\mathbf{M}_2 = \begin{bmatrix} 0 & i/\gamma_1 \\ i\gamma_1 & 0 \end{bmatrix}\begin{bmatrix} 0 & i/\gamma_2 \\ i\gamma_2 & 0 \end{bmatrix} = \begin{bmatrix} -\gamma_2/\gamma_1 & 0 \\ 0 & -\gamma_1/\gamma_2 \end{bmatrix} \tag{1.56}$$

Thus, $m_{11} = -\lambda_2/\lambda_1$, $m_{22} = -\lambda_1/\lambda_2$, $m_{12} = m_{21} = 0$

Using equation Eq. 1.51, the reflection coefficient (ρ) and reflectance (R) become:

$$\rho = \frac{\gamma_2^2\gamma_o - \gamma_2\gamma_1^2}{\gamma_2^2\gamma_o + \gamma_s\gamma_1^2} \tag{1.57}$$

$$R = \left(\frac{n_o n_2^2 - n_s n_1^2}{n_o n_2^2 + n_s n_1^2}\right)^2 \tag{1.58}$$

Thus, zero reflectance is obtained when $n_o\,(n_2)^2 = n_s\,(n_1)^2$, or $n_2/n_1 = (n_s/n_o)^{1/2}$. This ratio should be 1.23 in the case of glass substrates. For example, if the two layers are ZrO_2 ($n_2 = 2.1$) and CeF_3 ($n_1 = 1.65$), the ratio $n_2/n_1 = 1.27$ is quite close to the desired

ratio 1.23, and the reflectance equals 0.1 % which is almost zero. The performance of this combination is shown in Figure 1.6.

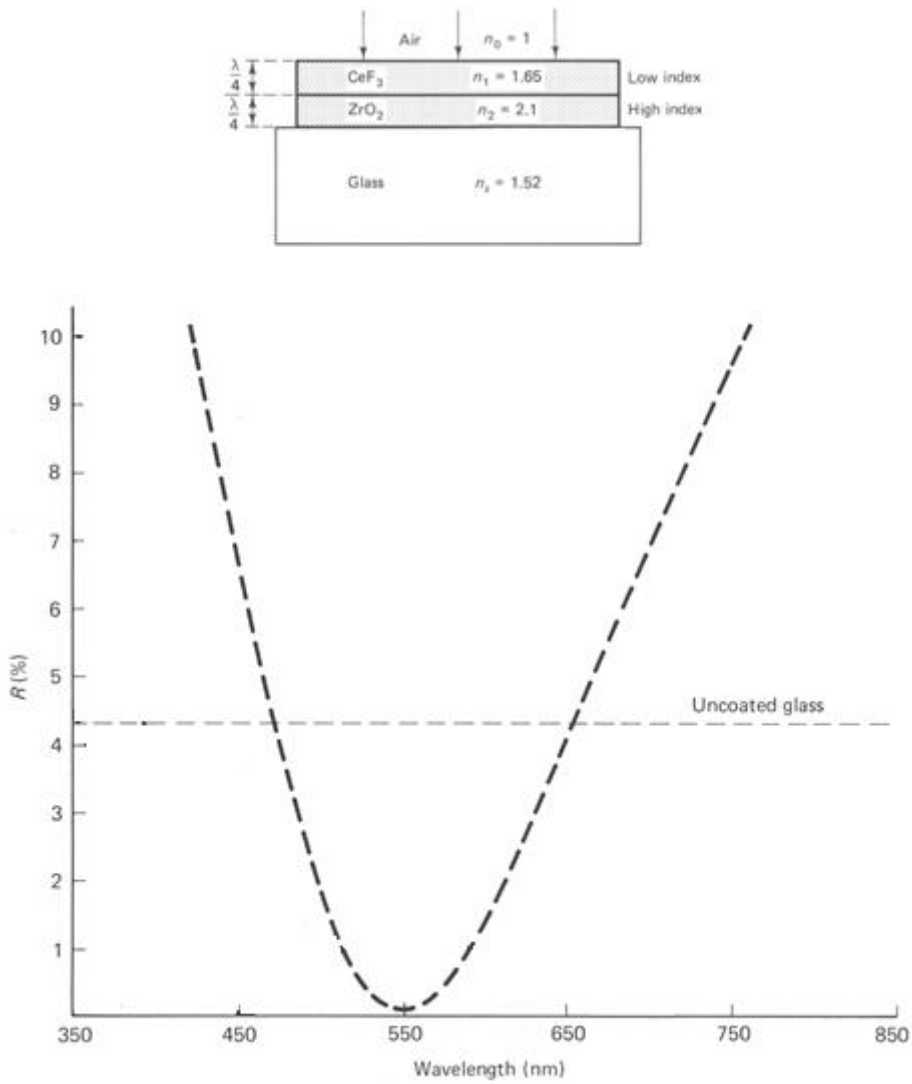

Figure 1.6: Reflectance from a double-layer film versus wavelength where n_o=1, n_s=1.52, n_1=1.65 and n_2=2.1. The two layers have the same thickness λ/4 where λ=550nm. [3]

1.3.4 Three-layer anti-reflecting films

The previous procedure was used to calculate the spectral reflectance of three-layer films. The use of coating with three or more layers makes possible a broader low-reflectance region in which the response is flatter. If each of the three layers is of *λ/4* thickness, one can show that a zero reflectance occurs when the refractive indices satisfy $\frac{n_1 n_3}{n_2} = \sqrt{n_0 n_s}$. For glass substrates, the ratio $\frac{n_1 n_3}{n_2}$ should be 1.23. A practical solution is shown in Figure 1.7.

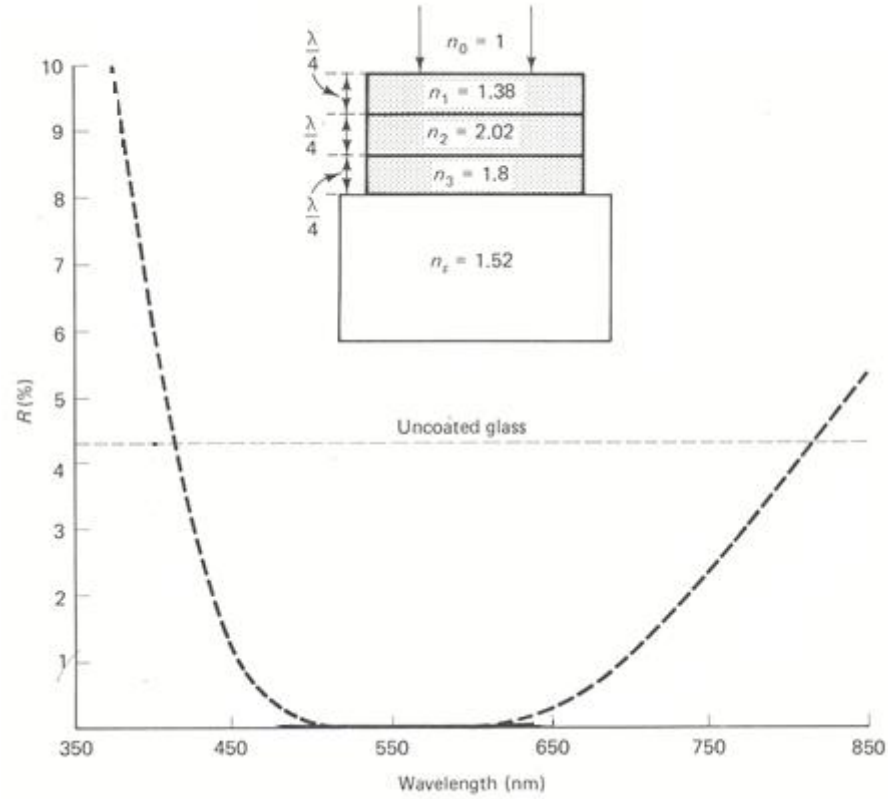

Figure 1.7: Reflectance from triple-layer films versus wavelength where n_o=1, n_s=1.52, n_1=1.38, n_2=2.02 and n_3=1.8. The three layers have the same thickness λ/4 where λ=550nm. [3]

1.4 Energy Efficient Coatings

An energy efficient coating is a type of a spectrally-selective coating which highly transmits the visible light and highly reflects the infrared (IR) heat. So, it is also called a transparent heat mirror. This topic has been studied heavily because it has a wide range of energy saving applications. One of the most beneficial applications is reflecting the solar heat in warm climates or preventing the escape of indoor heat in cold climates [4]. In addition, it can be used for coating furnace windows in order to observe samples under heat treatment from the outside [5]. Moreover, energy efficient coatings are used to improve the efficiency of incandescent lamps.

Energy efficient coatings can be classified into four main types. The first type is a thin metal film with high IR reflectance and low-enough visible absorption. The second type is obtained when a thin metal film is coated by one or several anti-reflecting dielectric layers. The third type is a single film of a semiconductor material with a sufficient wide bandgap to provide transparency in the visible region and a high-enough free carrier concentration to obtain IR reflectance. The last type is a conducting microgrid with appropriate opening sizes that are large enough to transmit the visible radiation but sufficiently small compared to IR wavelengths so that the microgrid can work as an IR reflector. The first two types are given more focus in the next sections. [6]

1.4.1 Thin metal films

Transparent heat mirrors should have two major characteristics: high visible transmittance (0.3-0.7μm) and high reflectance in the near IR region (0.7-2.5μm). Most

metals, especially noble metals (Ag, Au, Cu and Al), have very high IR reflectance due to their high free-electron concentration [7, 8]. Therefore, thin metal films can produce transparent heat mirrors if they show high transparency in the visible range. This can be attained by minimizing the reflectance and absorption in the visible range. It is reported that the absorption of the films is equal to $4\pi\ k\ d/\lambda$ where k, d and λ are the extinction coefficient, film thickness, and the wavelength, respectively [9]. Thus, the absorption is reduced by decreasing the film thickness. The visible reflectance can be minimized by destructive interference between the beams reflected from the front and back of the metal film, as shown in Figure 1.8. This destructive interference occurs when the contribution to the phase difference from the passage, through the metal, δ is negligible. The phase change δ is proportional to ($n\ d$) where n is the refractive index of a thin metal film and d is its thickness. Therefore, δ is negligible when the metal has a low refractive index in the visible range. In addition, the thickness of the film should be as thin as possible, provided that the film is continuous. Any discontinuity in the film affects the conductivity, and consequently it degrades the IR reflectance. [7,9]

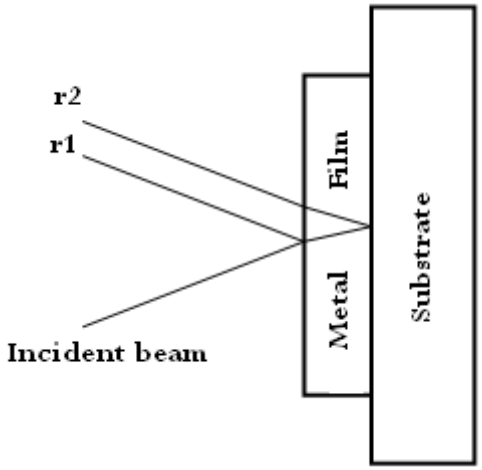

Figure 1.8: Geometry of light beams reflected from a metal film.

Now, let us investigate the selectivity of metals. It has been shown that noble metals are more selective than transition metals (Ni, Fe, Co and Cr). This is because of the low refractive index of noble metals compared to that of transition metals. For example, the refractive index of silver is around 0.06 at 550 nm, while that of Fe is about 2.7 at the same wavelength [7]. Silver is superior because it has the lowest refractive index and the lowest absorption in the visible range compared to Cu and Au [8,9]. Silver thin films are not stable, because of their high tendency to form an oxide overlayer which tremendously affects the IR reflectance [6-8]. Gold thin films are more stable than Ag and Cu due their inertness to the environment [8].

Thin metal films suffer from some major problems. The first problem is the strong tendency of metals to form island structures, particularly when the thickness is less than 15 nm [10]. This problem is overcome by depositing a nucleation modification dielectric layer between the metal and the substrate [8]. Another problem is that thin metal films

still do not offer high transmittance in the visible range simultaneously with high IR reflectance. The low visible transmittance (less than 60%) of Cu and Ag is shown in Figures 1.9 and 1.10. This is due to the high free-electron concentration of these metals [7]. Furthermore, thin metal films do not provide the stability and durability needed for practical heat mirrors [8]. The visible transmittance, stability and durability of metal films are enhanced by overcoating the metal with a dielectric layer [8]. This type of coating is discussed in the next section.

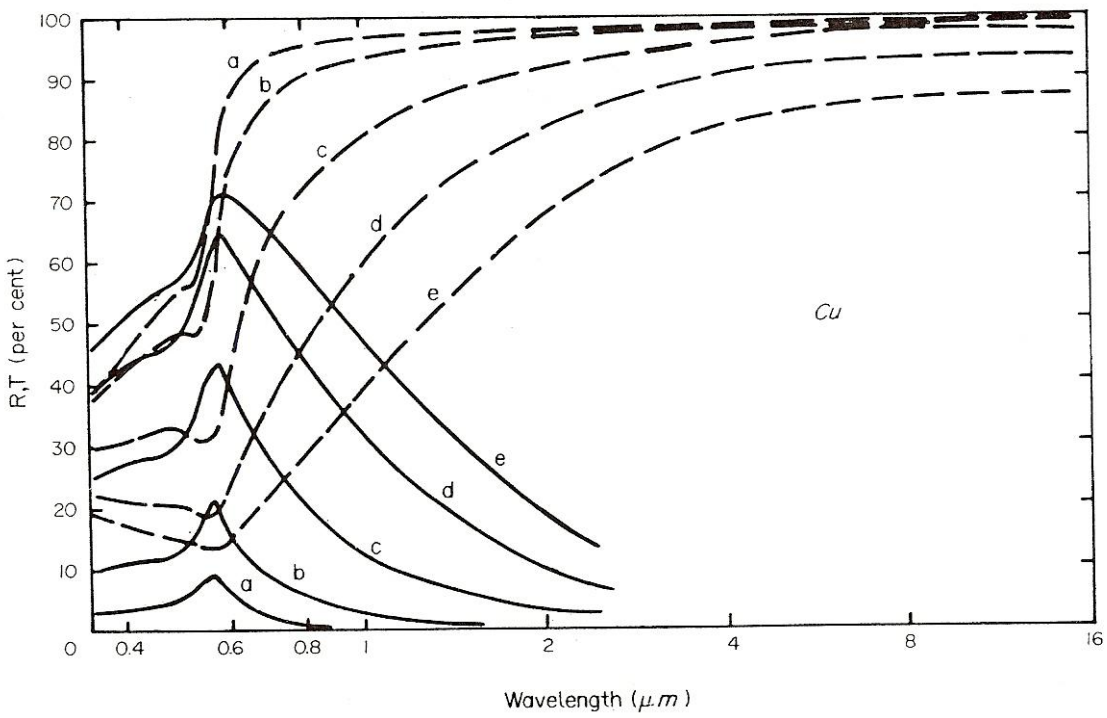

Figure 1.9: Reflectance (— —) and transmittance (———) of thin copper films on glass at different thicknesses: (a) 45nm, (b) 28nm, (c) 16nm, (d) 10nm and (e) 7nm. [7]

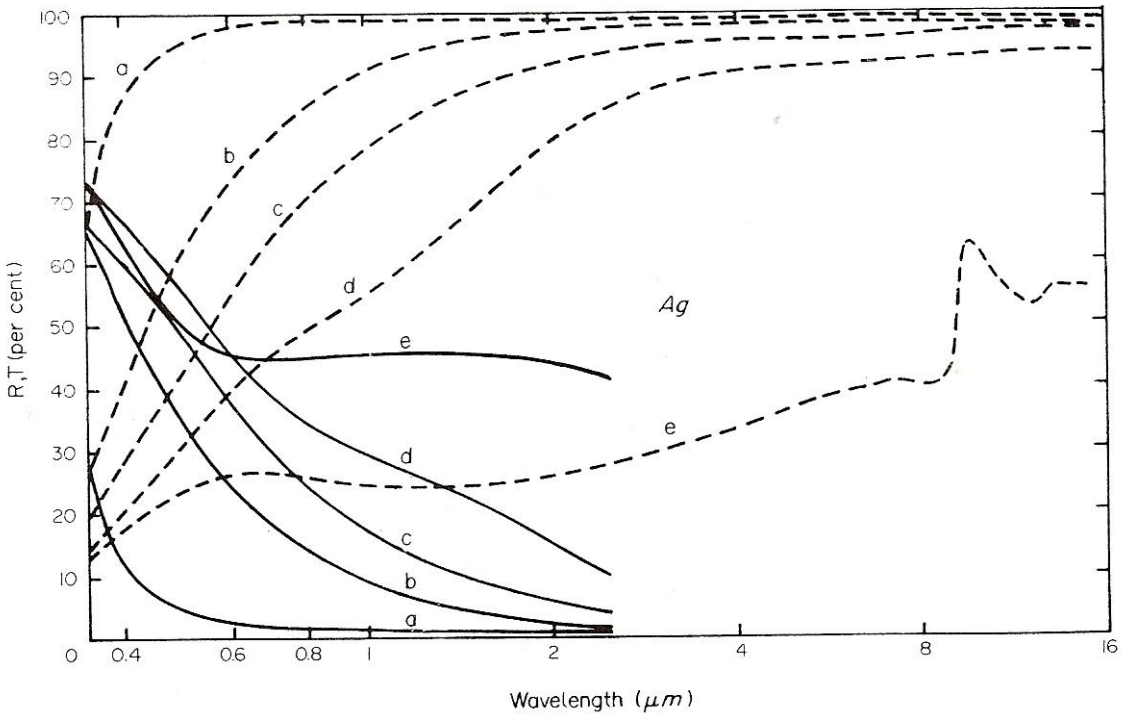

Figure 1.10: Reflectance (— —) and transmittance (———) of thin Ag films on glass at different thicknesses; (a) 36nm, (b) 16nm, (c) 12nm, (d) 9nm and (e) 6nm. [7]

1.4.2 Metal-dielectric multilayers

Transparent heat mirrors can be formed by sandwiching the metal layer between two dielectric layers as a three-layer Dielectric/Metal/Dielectric (D/M/D) coating. Using this type of coating, the stability, durability and visible transmittance are significantly improved. The top (outer) dielectric layer works as an anti-reflecting layer, which enhances the visible transmittance [10]. The best result for transparent heat mirrors is obtained when the two dielectric layers have the same thickness [11]. The metal layer works as an IR reflector and thus, it should be as thick as possible. The change in

thickness of the metal layer exercises a greater change in the optical properties of the coating than a change in the thickness of the dielectric layer [12]. It has been shown that the best performance of the D/M/D coating occurs when the refractive index of the dielectric layer (n_D) equals the extinction coefficient of the metal layer k_M [13]. In this case, the greatest possible metal thickness occurs when the dielectric thickness is given by $d=\lambda/8n_D$ where λ is the wavelength at which the maximum transmittance is desired [13]. However, most dielectrics have n_D less than k_M, and thus the dielectric thickness should be greater than that given by $d=\lambda/8n_D$. The lowest possible value of the dielectric refractive index for an acceptable transparent coating is about 1.96 [11]. The D/M/D structure has been widely used for the production of energy-efficient coatings because of its distinct advantages over single metallic films. Table 1.3 summarizes the reported D/M/D energy efficient coatings.

Table 1.3: Summary of the reported D/M/D energy efficient coatings.

Group	Structure	Method	Reference
J. Fan et al.	$TiO_2/Ag/TiO_2$	Rf sputtering	[15]
J. K. Fu et al.	$TiO_2/Ag/TiO_2$	Plasma ion assisted deposition	[16]
X. Zhang et al.	ZnS/Ag and ZnS/Al	Thermal evaporation	[17]
G. Leftheriotis et al.	ZnS/Ag/ZnS	Thermal evaporation	[11,14]
H. Kostlin et al.	ZnS/Ag/ZnS	Thermal evaporation	[13]
D.R. Sahu et al.	ZnO/Ag/ZnO	simultaneous DC (Ag) and RF (ZnO) magnetron sputtering	[18]
D.R. Sahu et al.	ZnO/Cu/ZnO	simultaneous DC (Cu) and RF (ZnO) magnetron sputtering	[19]
J. George et al.	$Bi_2O_3/Au/Bi_2O_3$	Activated reactive evaporation	[20]
P. Jin et al.	$TiO_2/TiN/TiO_2$	Sequential sputtering	[4]
M. Okada et al. Q.-N. Zhao et al.	$TiO_2/TiN/TiO_2$	Reactive magnetron sputtering	[21, 22]
C-K. Jung et al	$TiO_2/TiN/TiO_2$	Pulsed dc sputtering	[23]
K. Andersson	$ZrO_2/ZrN/ZrO_2$	Reactive magnetron sputtering	[24]

1.5 Scope of the Work

In the present study, two-layer (D/M/substrate) and three-layer (D/M/D/substrate) transparent heat mirrors were fabricated by using thermal evaporation, and their optical properties were investigated. The metals were silver and gold, while the dielectric was tungsten oxide (WO_3). Tungsten oxide was chosen because it has the basic requirements of the dielectrics used in transparent heat mirrors, namely its wide band gap of 3.25 eV which provides visible transparency and its high refractive index (around 2.02). In this study, the effect of the metal thickness on the performance of WO_3-based transparent heat mirrors was investigated.

Chapter 2: EXPERIMENTAL DETAILS

2.1 Sample Preparation

Thin films were prepared, using thermal evaporation in a vacuum around 5×10^{-5} mbar, by means of a Leybold model L560 box coater pumped by a turbomolecular pump. Molybdenum boats were used for the evaporation of silver (Ag) and tungsten oxide (WO_3), while tungsten boats were used for evaporation of gold (Au). The starting materials were powders of WO_3 (Alfa Aesar, 99.8 % purity), silver (Alfa Aesar, 99.999 % purity) and solid pieces of gold (99.999% purity). The substrates were unheated to avoid the diffusion between the layers. The source-to-substrate distance was 40 cm. In order to produce films with uniform thickness, the substrates were rotated during the deposition. The thicknesses of the films were monitored and controlled by a quartz crystal thickness monitor and rate controller. The evaporation rate of the dielectric (WO_3) was 0.4 nm/s while the evaporation rate of the metals (Ag and Au) was 1.0 nm/s. Various single layer, two layers and three layers were fabricated. The single layer was either Ag, Au or WO_3. The two and three layers were: WO_3/Ag, WO_3/Au, WO_3/Ag/WO_3 and WO_3/Au/WO_3. Both two and three layers were fabricated in one experiment without breaking the vacuum. Therefore, two different evaporation sources were required. The designed parameters used for thicknesses of the films are shown in Table 2.1.

Table 2.1: Designed parameters used for thickness of the films.

Materials	Thickness (nm)	
	Single film	Multilayer coatings
WO_3	35	35 and 70
Ag	11 and 18	18, 25, 32 and 39
Au	12 and 16	20, 28, 36 and 44

2.2 Films Characterization

After the films were deposited, they were removed from the coating chamber, and various characterization techniques were employed to study their respective properties. The normal-incidence transmittance (T) and reflectance (R), of the films deposited on fused silica substrates, were measured, over the wavelength range from 200 to 2000 nm, by using a JASCO V570 spectrophotometer. Samples were maintained at room temperature and pressure for around one year, and then the normal-incidence *R* and *T* were measured again.

The chemical composition of the films was studied by using x-ray photoelectron spectroscopy (XPS), and it was performed in a VG Scientific ESCALAB MKII spectrometer equipped with an Al K_α (1486.6 eV) x-ray source. The instrumental resolution was 1.2 eV with a slit width of 0.6 cm. Prior to the XPS analysis, the samples were transferred in air to the XPS analysis chamber. During the XPS analysis, the samples were maintained at ambient temperature at a pressure of 5×10^{-7} Pa. Chemical

depth profiles of the films were obtained by a sequence of etching followed by XPS measurement. Etching was performed by using a 4-keV Ar+ ion beam. During depth profiling, the chamber pressure was 10^{-5} Pa, and the ion current, at the sample surface, was 1.2 μA. The XPS showed that our films were sub-stoichiometric.

The surface morphology of the films was examined by the tapping mode AFM (Veeco Innova diSPM). The sample surface was probed with a silicon tip of 10 nm radius oscillating at its resonant frequency of 300 kHz. The scan area was 2×2 μm^2, and the scan rate was 1 Hz.

The thicknesses of the films were measured using a stylus surface profilometer (Ambiox XP-2), with an error of less than 10%.

Chapter 3: SINGLE FILMS

3.1 Silver (Ag) Films

3.1.1 AFM of silver films

The AFM technique was used to study the morphology of two silver films having thicknesses of 11 and 18 nm. These films were deposited on glass substrates. It is obvious from Figure 3.1 that the silver film of thickness 11 nm was at the nucleation stage forming an island structure of silver on the substrate. However, the silver film of thickness 18 nm showed a continuous and uniform 3D structure, as shown in Figure 3.2. Thus, it can be concluded that silver films of thicknesses 18 nm were continuous. These results agree with the reported minimum thickness for continuous silver films, which is 12 nm [16]. For transparent heat mirrors, the metal layer has to be continuous. Otherwise the IR reflectance degrades. Thus, the thicknesses of the silver layers, in WO_3/Ag/WO_3 and WO_3/Ag multilayers, were 18 nm.

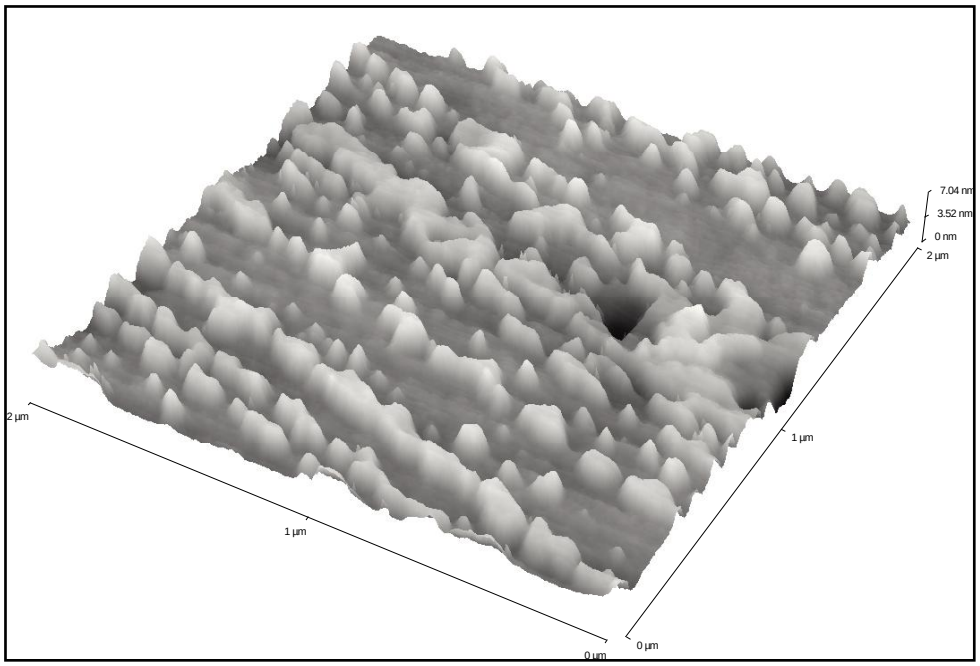

Figure 3.1: 3D AFM image of a silver film with a thickness of 11 nm, deposited on a glass substrate. It shows a discontinuous silver film.

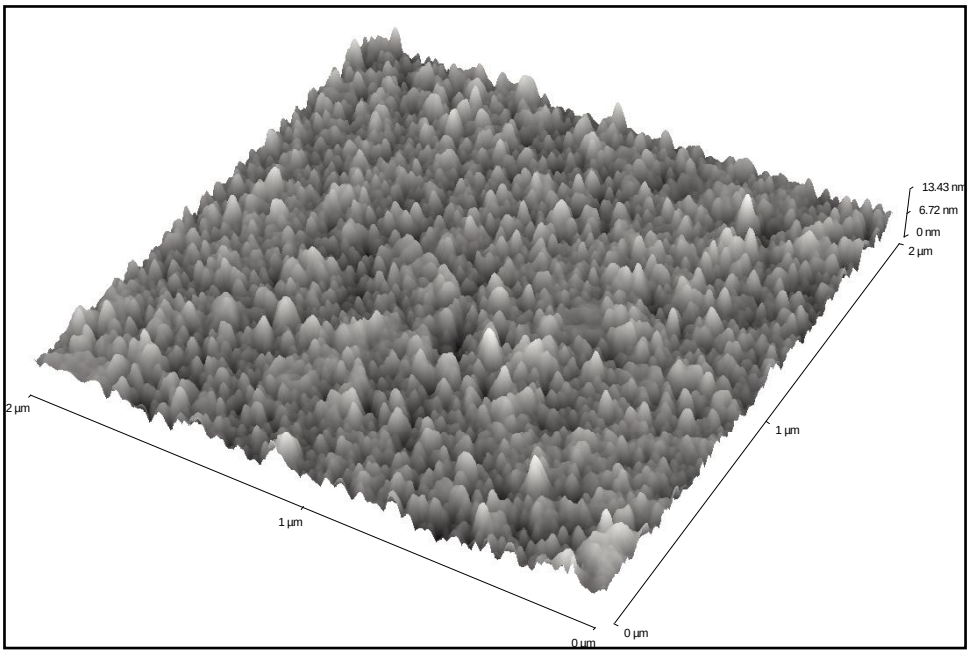

Figure 3.2: 3D AFM image of a silver film with a thickness of 18 nm, deposited on a glass substrate. It shows a continuous silver film.

3.1.2 Reflectance and transmittance of silver films.

The reflectance and transmittance of silver films were measured for different thicknesses: 11, 18, 25, 32 and 39 nm. All films were deposited on fused silica substrates. Figures 3.3 and 3.4 show the visible transmittance and infrared reflectance of silver, respectively. The transmittance peak occured at a wavelength of ~350 nm, which is in the near ultraviolet region. The reflectance increased as the thickness of the silver layer increased, whereas the transmittance showed the opposite trend. The IR reflectance dropped dramatically when the thickness changed from 18 to 11 nm.

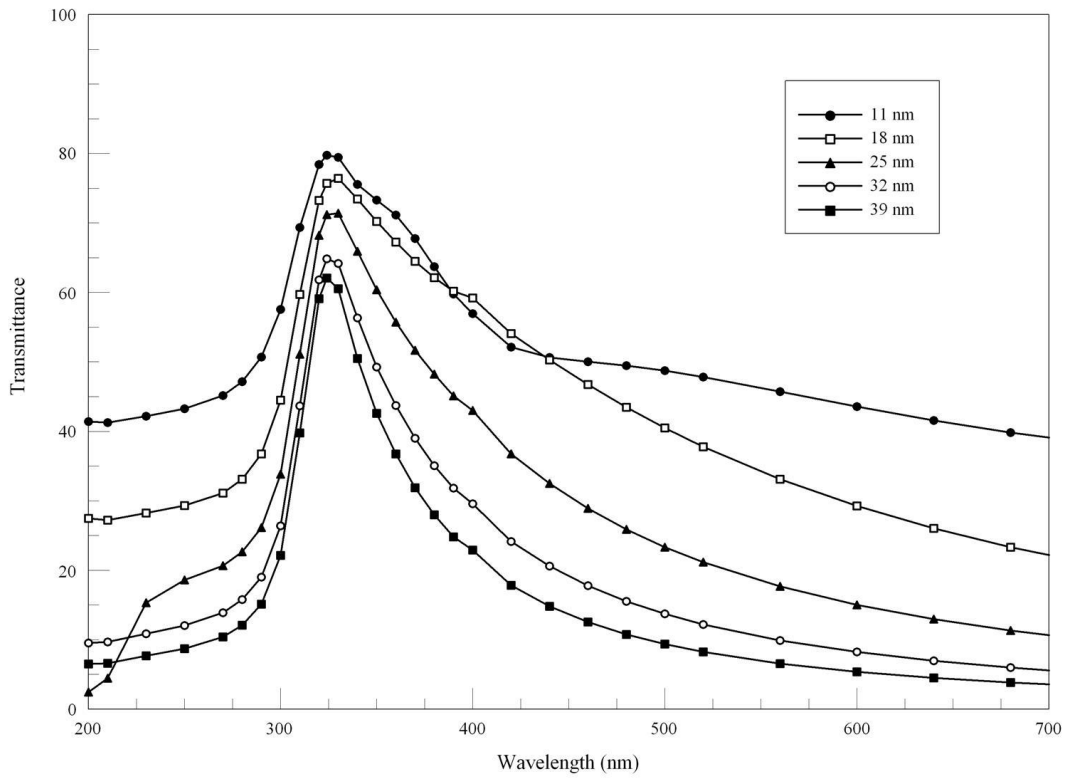

Figure 3.3: Visible transmittance of different thicknesses of silver films deposited on fused silica substrates.

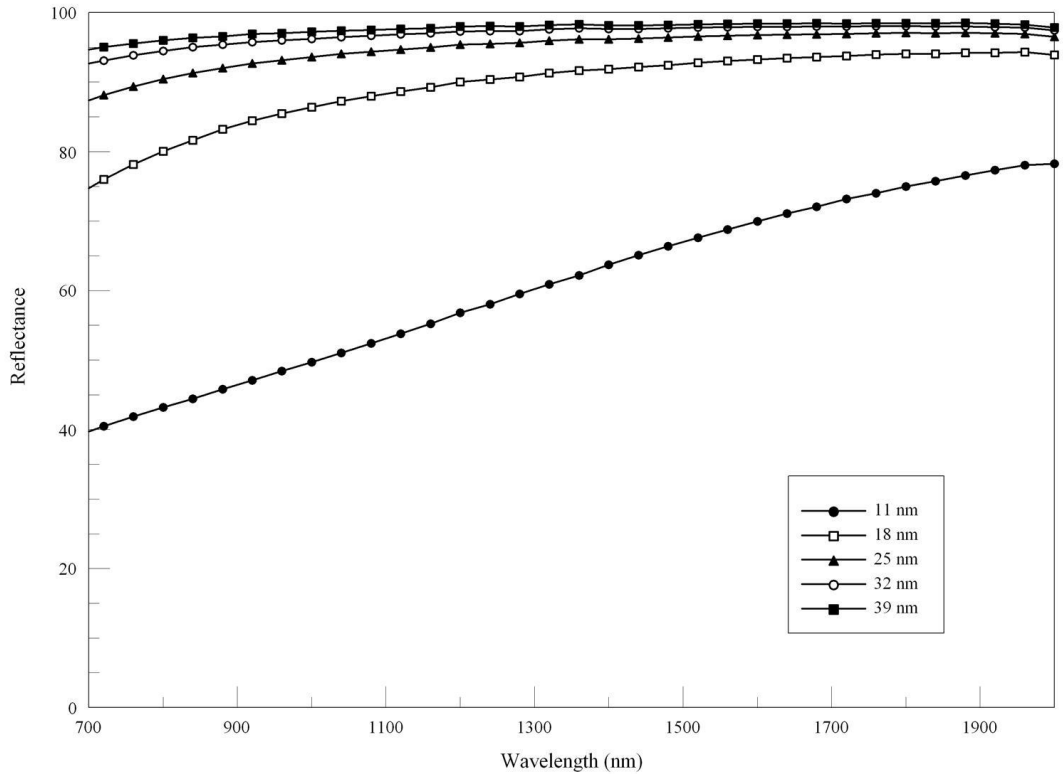

Figure 3.4: Infrared reflectance of different thicknesses of silver films deposited on fused silica substrates.

3.2 Gold (Au) Films

3.2.1 AFM of gold films

The surfaces of two films of gold were studied by using the AFM technique. The two films were deposited on glass substrates, and they had thicknesses of 12 and 16 nm. The images are shown in Figures 3.5 and 3.6. The AFM images show that the gold films were continuous for both thicknesses. In the WO_3/Au/WO_3 and WO_3/Au multilayers, the thicknesses of the gold were 20 nm. According to the AFM results, such gold films were continuous.

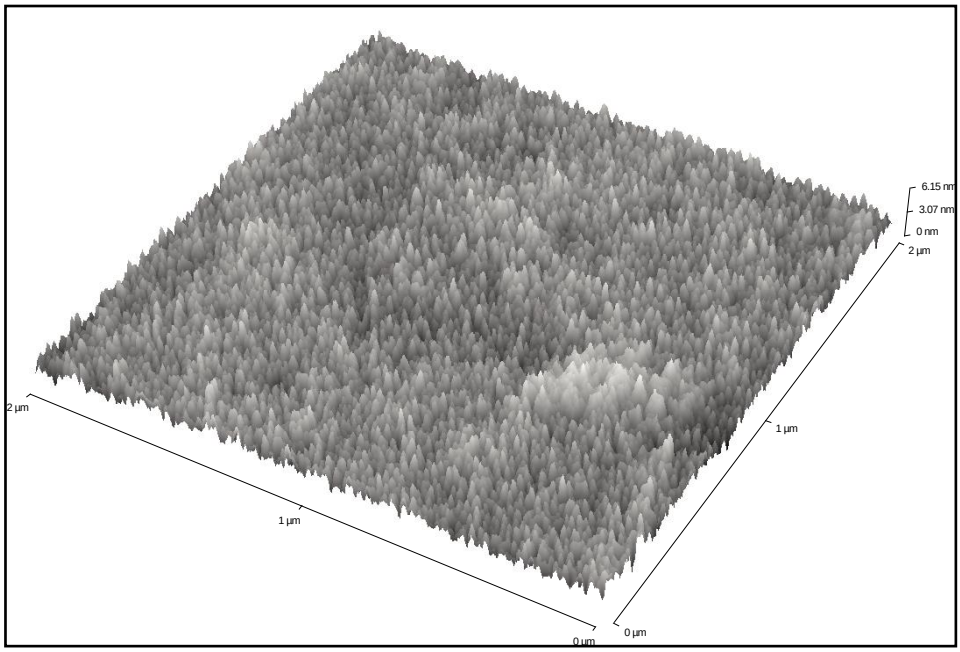

Figure 3.5: 3D AFM image of a gold film with a thickness of 12 nm, deposited on a glass substrate. It shows a continuous gold film.

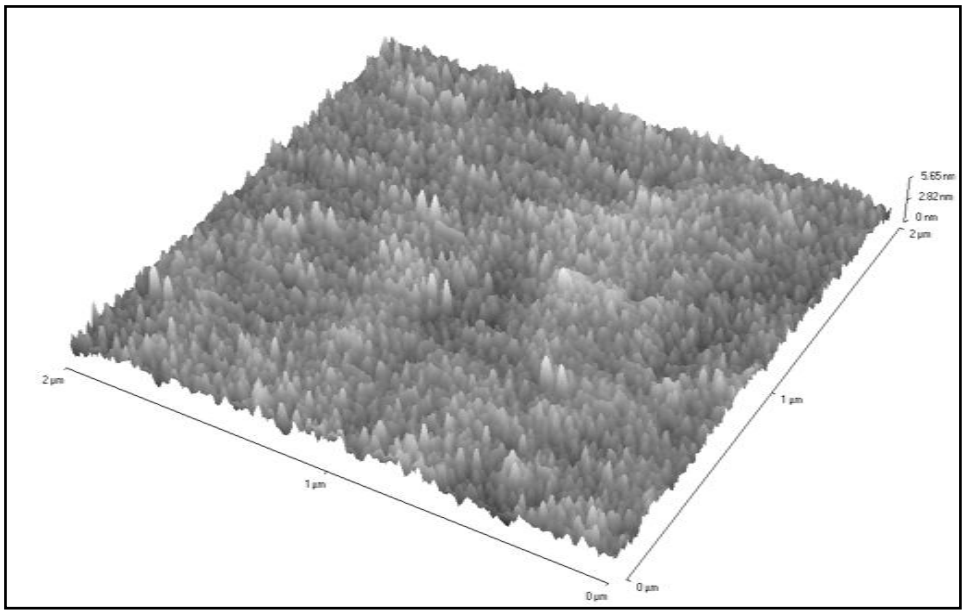

Figure 3.6: 3D AFM image of a gold film with a thickness of 16 nm, deposited on a glass substrate. It shows a continuous gold film.

3.2.2 Reflectance and transmittance of gold films

The reflectance and transmittance were measured for gold films deposited on fused silica substrates. Figures 3.7 and 3.8 show the visible transmittance and infrared reflectance spectra for different thicknesses of gold: 12, 20, 28, 36 and 44 nm. The transmittance peak occured at a wavelength of ~510 nm, which is in the visible region. The reflectance increased as the thickness of the gold layer increased, whereas the transmittance showed the opposite trend.

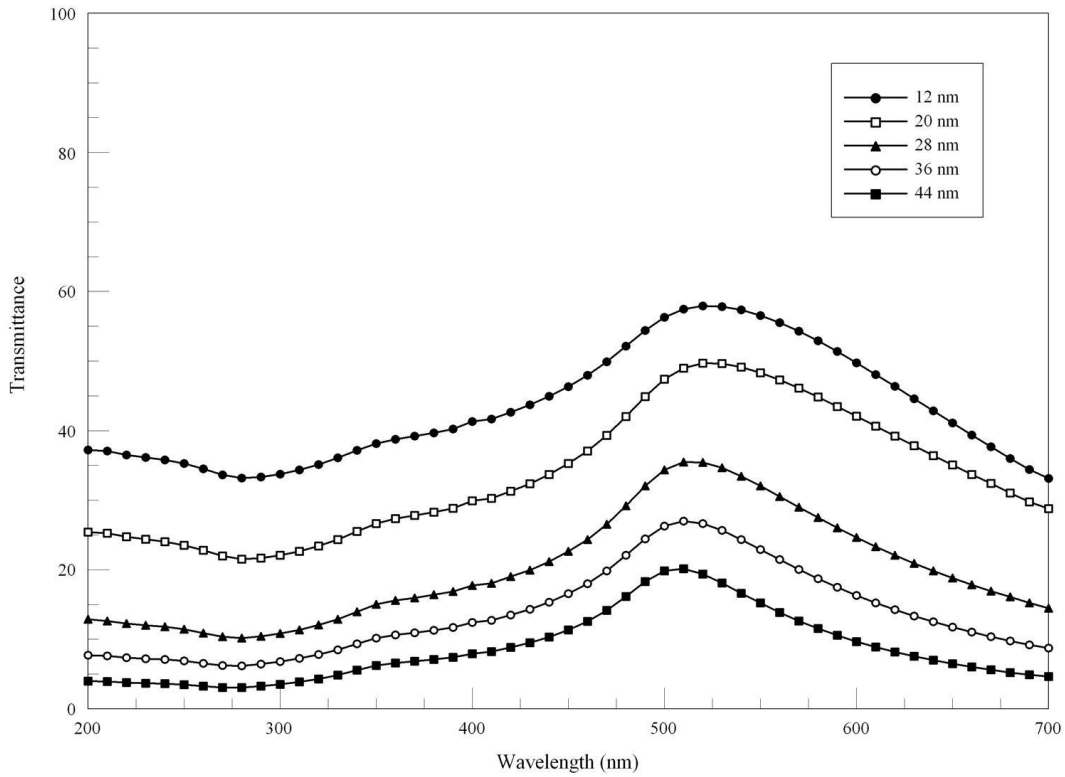

Figure 3.7: Visible transmittance of different thicknesses of gold films deposited on fused silica substrates.

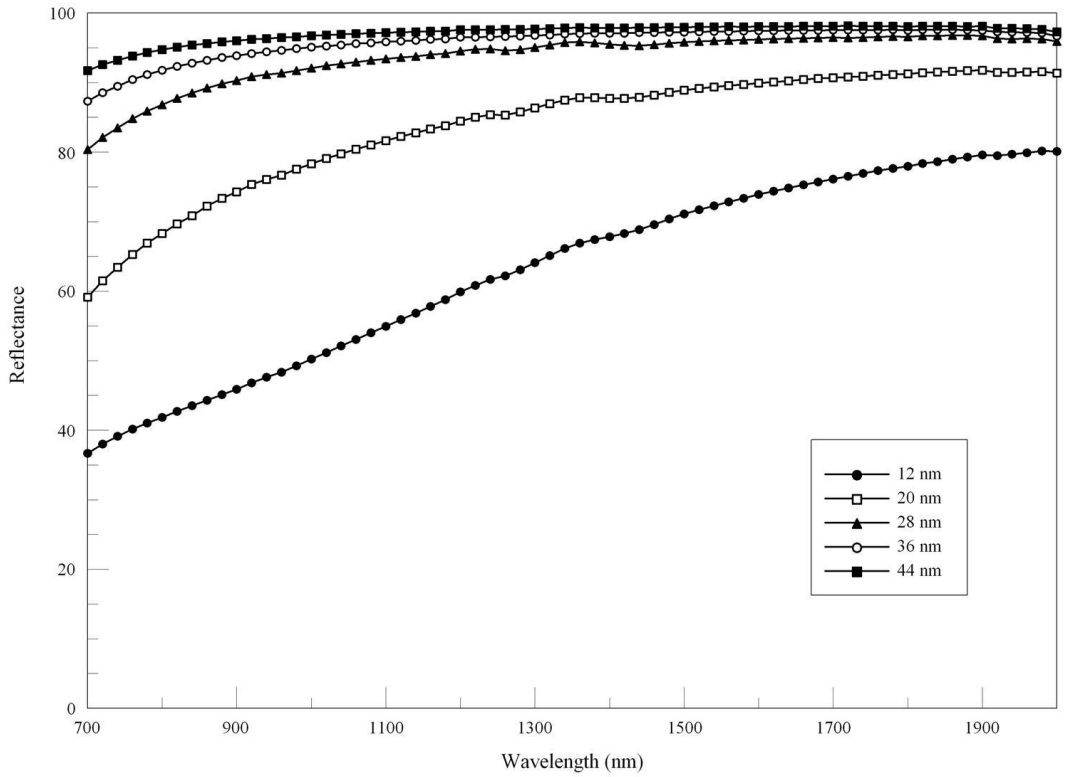

Figure 3.8: Infrared reflectance of different thicknesses of silver films deposited on fused silica substrates.

3.3 Tungsten Oxide (WO_3) Films

3.3.1 AFM of a WO_3 film

The morphology of a WO_3 film was investigated by using AFM. The film was deposited on glass with a thickness of 35 nm, and the image is shown in Figure 3.9. It can be concluded from the image that the film of WO_3 was dense with a smooth surface and a granular structure. Therefore, it will not cause much light scattering, which is an undesired process in the energy-efficient coating.

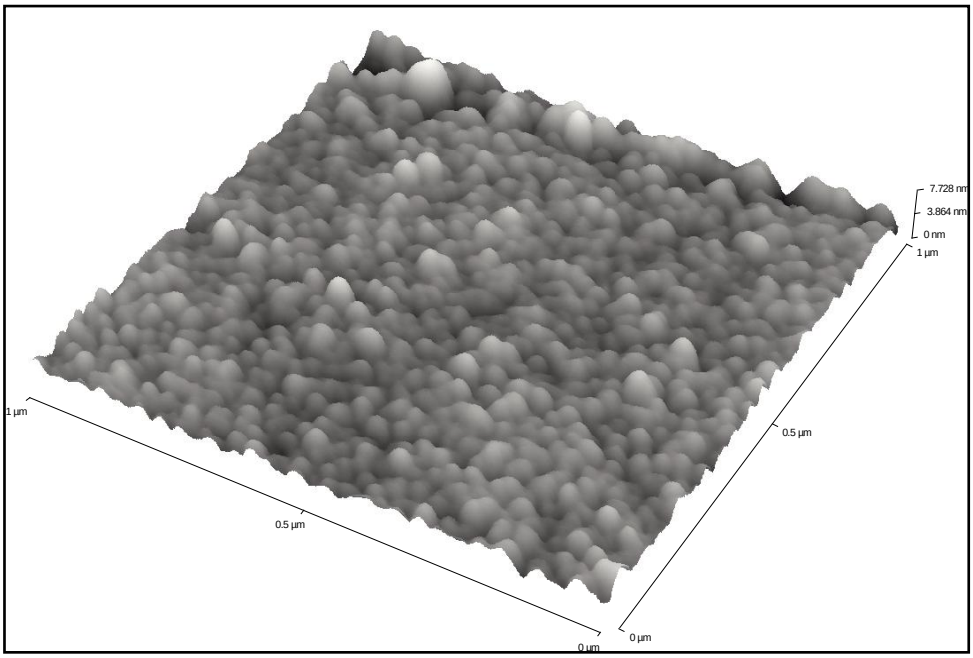

Figure 3.9: 3D AFM image of a tungsten oxide film with a thickness of 35 nm, deposited on a glass substrate. The film was dense with a smooth surface and a granular structure.

3.3.2 Determination of the optical constants of WO_3 films

A method for the determination of the refractive index (n) and extinction coefficient (k) of thin dielectric films on transparent substrates, with refractive index n_s, were reported earlier by Denton [25]. It requires measurements, at normal incidence, of the reflectance and transmittance of the film on the substrate. The normal-incidence reflectance and transmittance spectra of a typical tungsten oxide thin film are shown in Figure 3.10. Then, R and T may be written in functional form as:

$$R = f_1(n, k, n_s, \lambda, d)$$

$$T = f_2(n, k, n_s, \lambda, d)$$

If the R and T of the film are measured as functions of λ, with known value of n_s and d, then, in principle, n and k can be determined from the above relations for R and T. There is no explicit expression for n or k [25]. However, the equations for R and T can be solved numerically to give values of n and k as functions of wavelength [25]. A procedure was given in [25] for determining the correct solutions for n and k, and also accurately fixing the film thickness. By adjusting the thickness, a solution can then be obtained, yielding a continuous dispersion curve quite distinct from unacceptable solutions [25]. The $n(\lambda)$ and $k(\lambda)$ curves are presented in Figures 3.11 and 3.12, respectively.

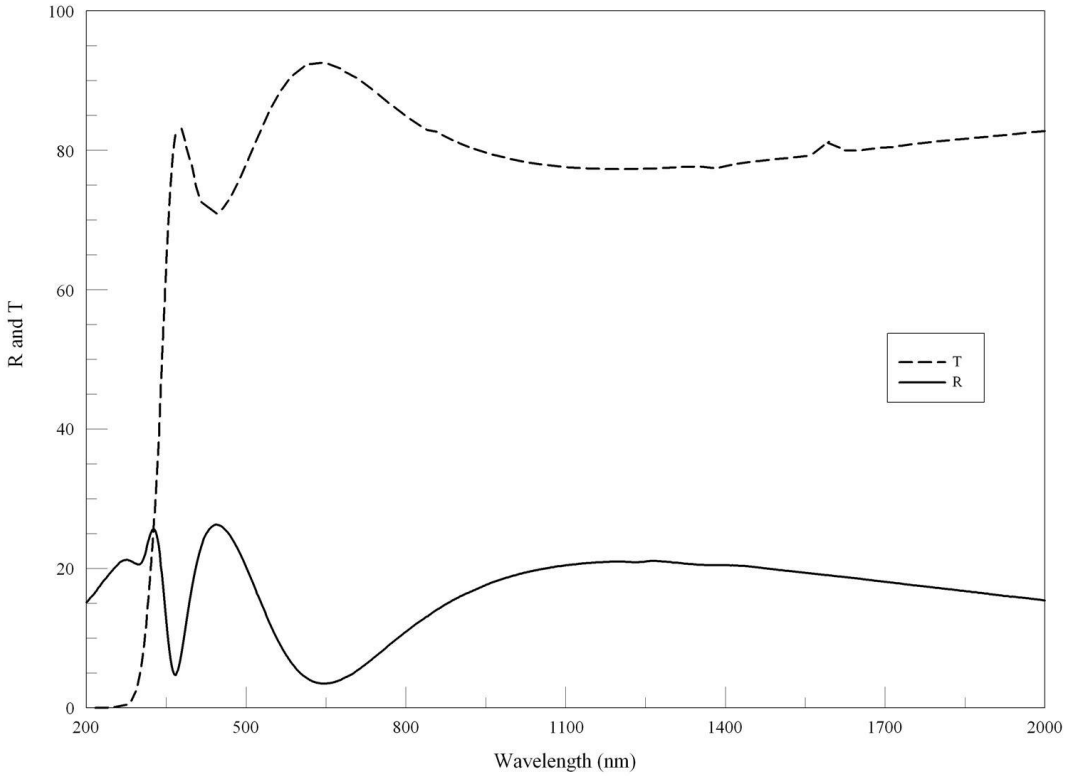

Figure 3.10: Optical spectra of a tungsten oxide thin film with a thickness of 152 nm.

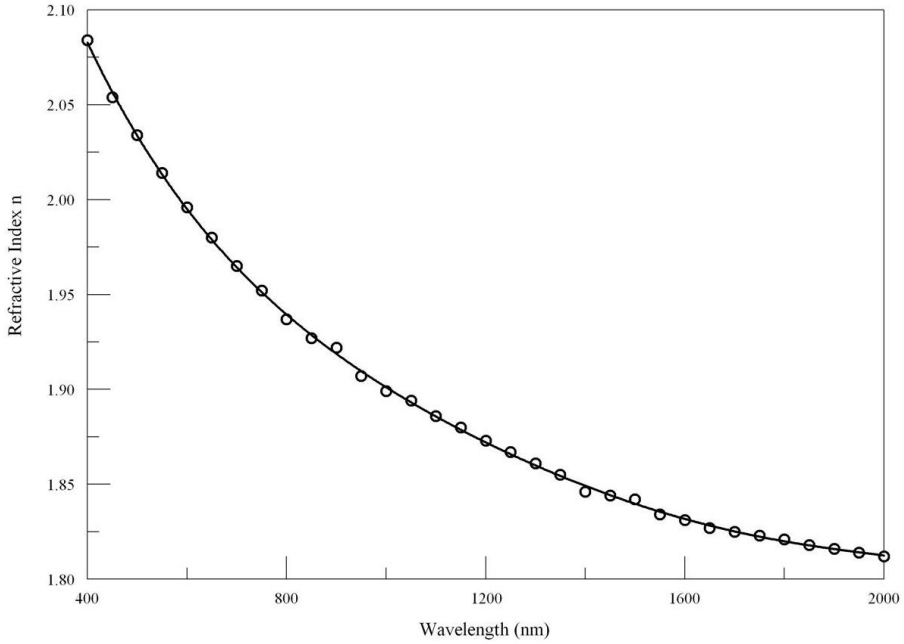

Figure 3.11: Refractive index of a WO_3 film, of thickness 152 nm, as function of wavelength.

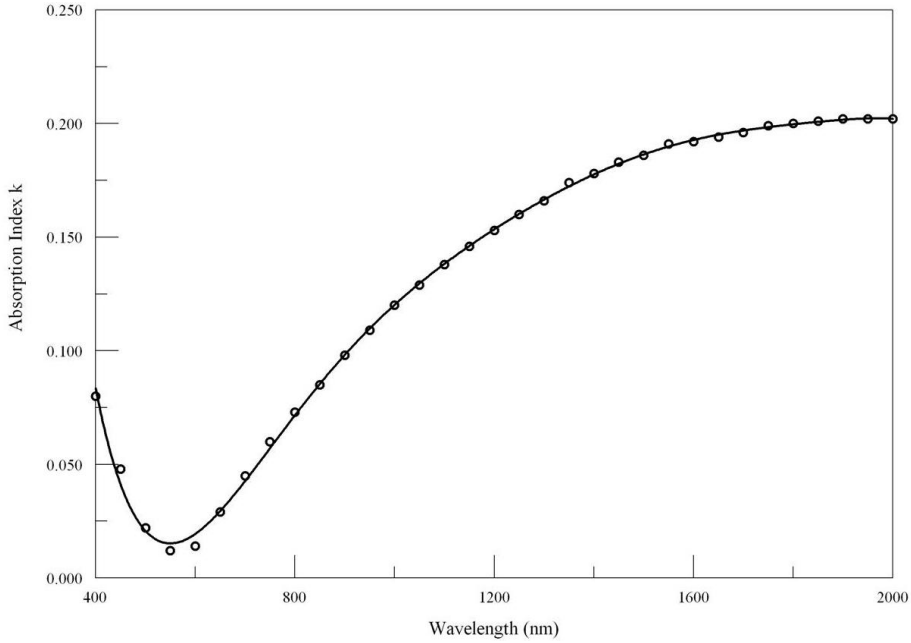

Figure 3.12: Extinction coefficient of a WO_3 film, of thickness 152 nm, as function of wavelength.

In the visible region, the average refractive index of WO_3 is about 2.02, and this is close to that of TiO_2 (n = 2.27) [26], which is widely used as a dielectric in multilayer transparent heat mirrors. The extinction coefficient in the visible region was ~0.04. This indicates minimum absorption in the visible range, which is a desirable property for the dielectric layers in a transparent heat mirror. However, the value of k is slightly large, approaching 0.2, in the infrared region. This is not appropriate for transparent heat mirrors since the absorption will become significant in the *IR* region. The reported reason for this increase in absorption is the formation of an absorption band by the defects, originating from oxygen vacancies in sub-stoichiometric films [27]. It has been shown that tungsten oxide thin films evaporated without oxygen atmosphere are sub-stoichiometric [28].

Chapter 4: SILVER-BASED MULTILAYER COATINGS

As illustrated in the theory, getting a good transparent heat mirror requires the thickness of the dielectric to be greater than $\lambda/8n_D$, where λ is the wavelength corresponding to minimum reflectance, and n_D is the refractive index of the dielectric at that wavelength. In the case of WO_3, at the center visible wavelength λ =550 nm, n_D equals 2.014. Therefore, the thickness of WO_3 layers must be greater than 34 nm. In this study, two thicknesses of WO_3 were investigated. The first thickness was 35 nm, which is the lowest possible thickness. This thickness produced high-quality transparent heat mirrors whose properties will be presented in chapters 4 and 5. The second thickness (70 nm) did not produce suitable heat mirrors, and its results are presented in Appendix A for comparison.

In this chapter, the transmittance and reflectance of the multilayer coatings WO_3/Ag/WO_3 and WO_3/Ag are presented. The thickness of the WO_3 layer was 35 nm while that of the Ag layer had different thicknesses: 18, 25, 32 and 39 nm. A figure of merit is used to evaluate the performance of these transparent heat mirrors.

4.1 Reflectance and Transmittance of Two-Layer (WO_3/Ag) Coating

The transmittance and reflectance spectra of two-layer WO_3/Ag coatings are shown in Figures 4.1-4.4 for different values of the thickness of the silver layer. These films did not show the desired properties of a transparent heat mirror, namely high visible transmittance along with high IR reflectance.

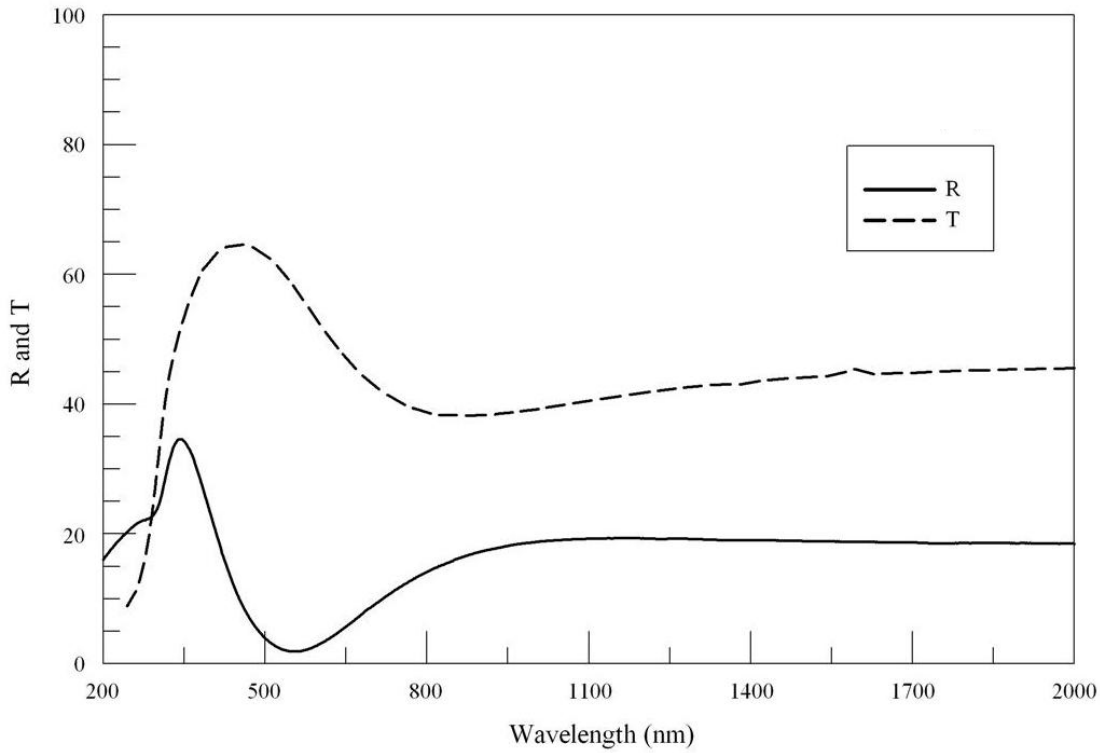

Figure 4.1: Reflectance and transmittance of WO_3/Ag coatings of thicknesses 35/18 (nm). The film was deposited on fused silica substrate.

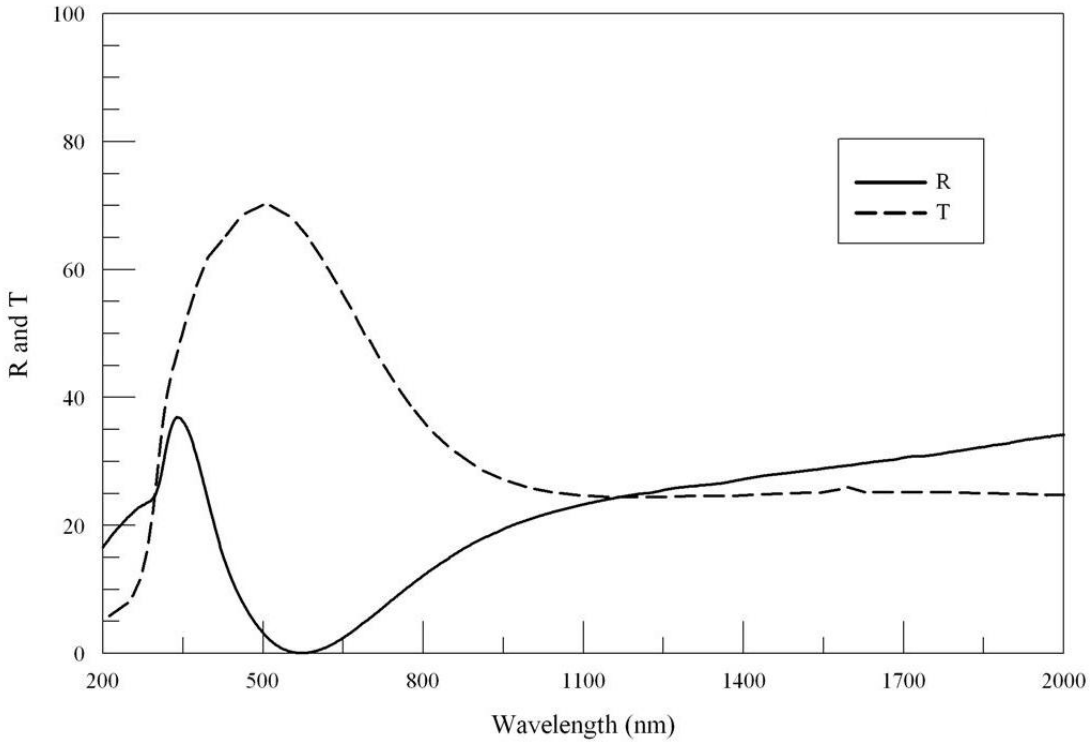

Figure 4.2: Reflectance and transmittance of WO_3/Ag coatings of thicknesses 35/25 (nm). The film was deposited on fused silica substrate.

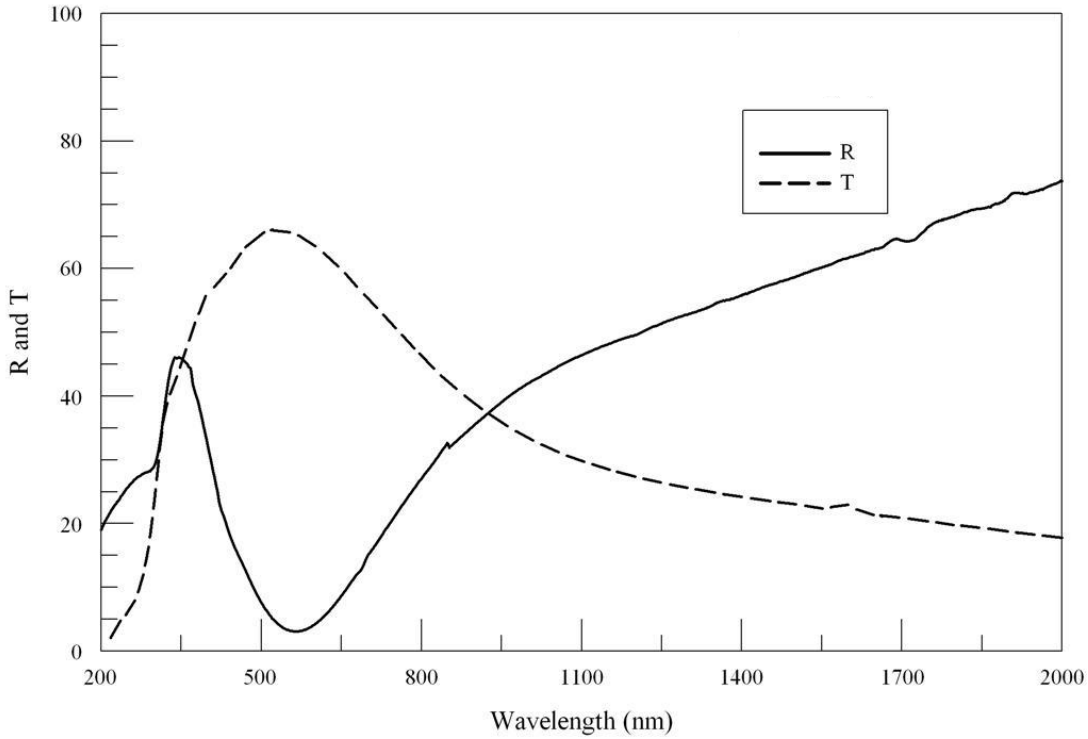

Figure 4.3: Reflectance and transmittance of WO_3/Ag coatings of thicknesses 35/32 (nm). The film was deposited on fused silica substrate.

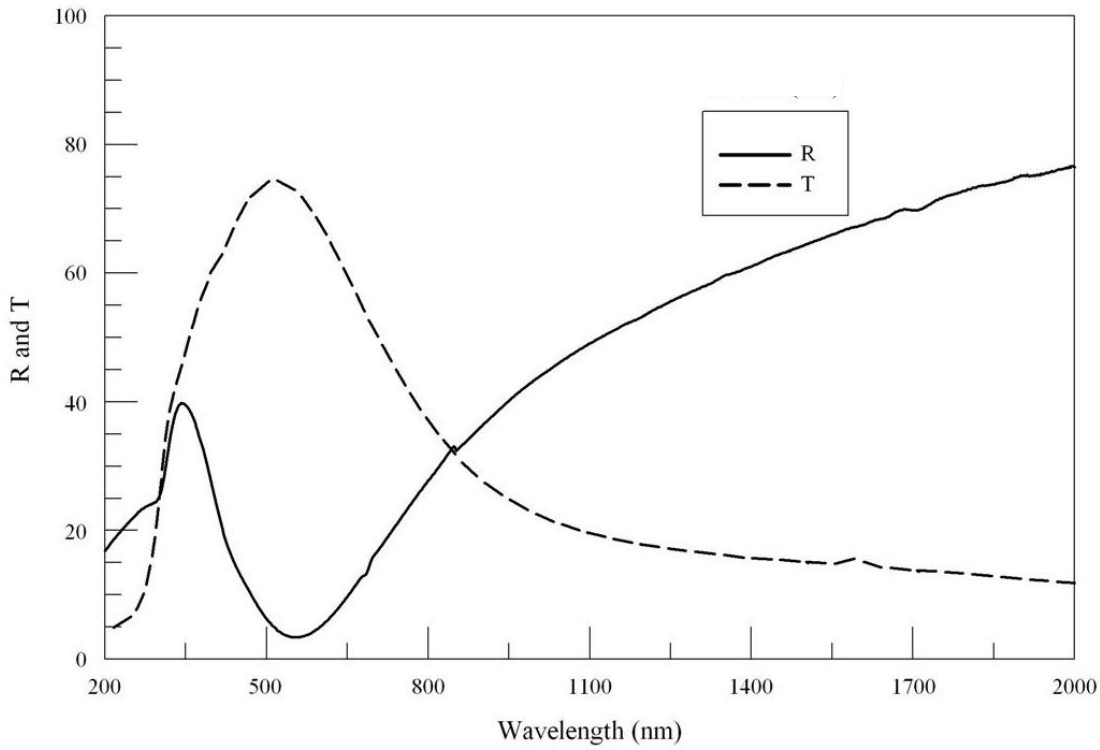

Figure 4.4: Reflectance and transmittance of WO_3/Ag coatings of thicknesses 35/39 (nm). The film was deposited on fused silica substrate.

4.2 Reflectance and Transmittance of Three-Layer (WO_3/Ag/WO_3) Coatings

The transmittance and reflectance spectra of three-layer WO_3/Ag/WO_3 coatings are shown in Figures 4.5-4.8 for different values of the thickness of the silver layer. A heat mirror with a very thin silver layer (Figure 4.5) did not exhibit the required selectivity. Selectivity was improved as the thickness of the silver layer increased. For thicker films (25 nm), the following observations can be made:

(i) The transmittance was largely confined to the visible range.

(ii) The band width of the transmittance narrowed as the thickness of the silver layer increased.

(iii) The maximum transmittance decreased as the thickness of the silver layer increased.

(iv) The infrared reflectance progressively increased as the thickness of the silver layer increased.

(v) The minimum reflectance was obtained for a wavelength around 500 nm. This wavelength shifted to lower values as the thickness of the silver layer increased.

These observations are consistent with the results on heat mirrors fabricated by using other dielectrics, such as ZnS [11] and TiO_2 [12]. The maximum visible transmittance was 88.3% at λ = 554 nm, and was obtained for the heat mirror with a silver layer thickness of 25 nm. This value is among the highest reported values for transparent heat mirrors.

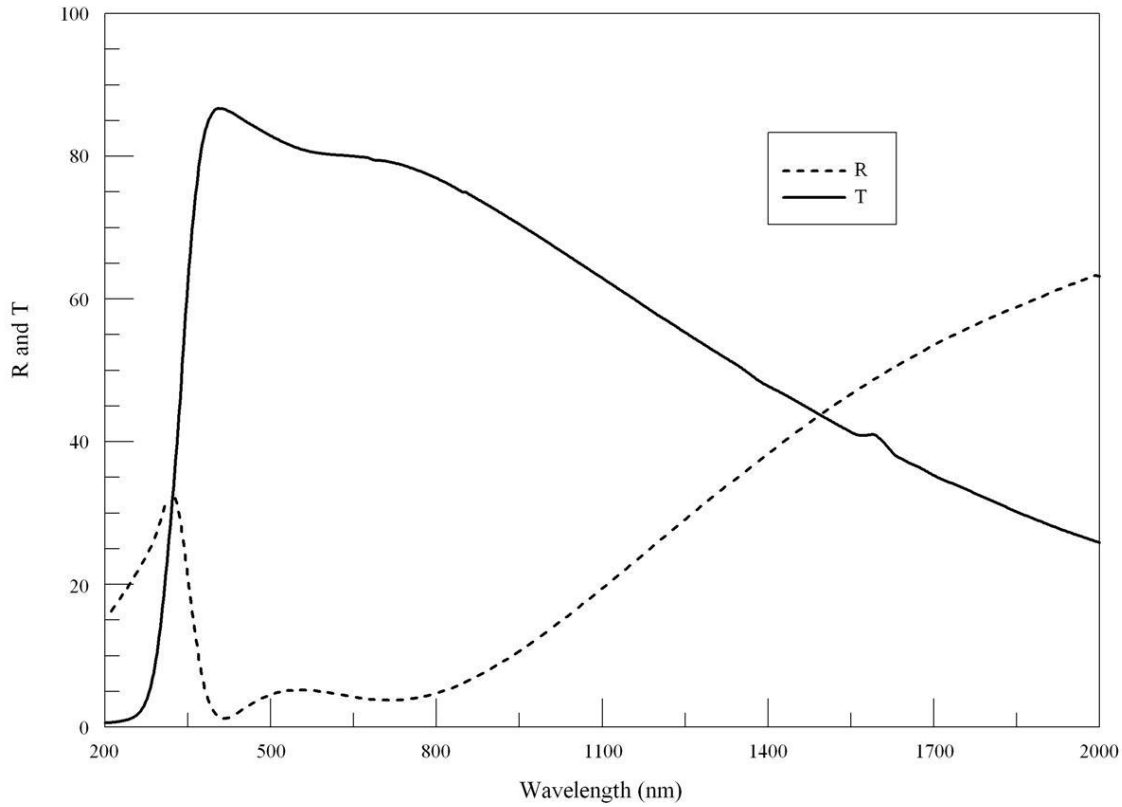

Figure 4.5: Reflectance and transmittance of WO_3/Ag/ WO_3 coatings of thicknesses 35/18/35 (nm). The film was deposited on fused silica substrate

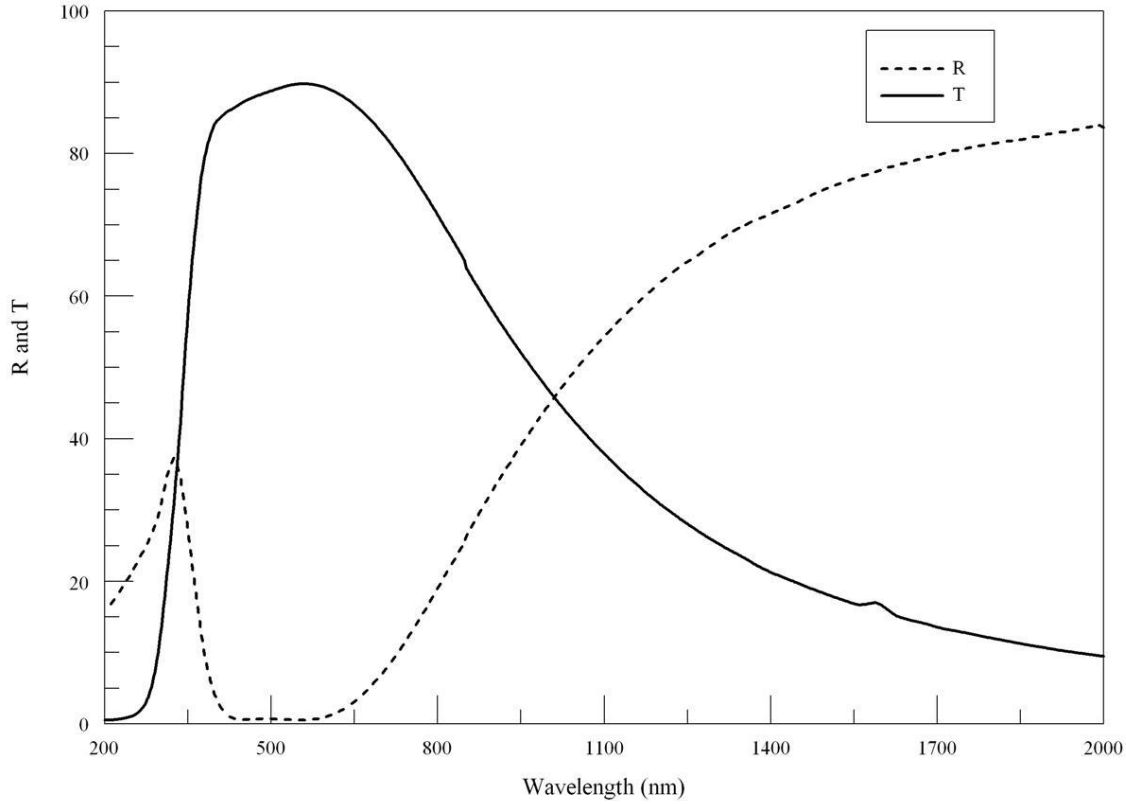

Figure 4.6: Reflectance and transmittance of WO_3/Ag/ WO_3 coatings of thicknesses 35/25/35 (nm). The film was deposited on fused silica substrate.

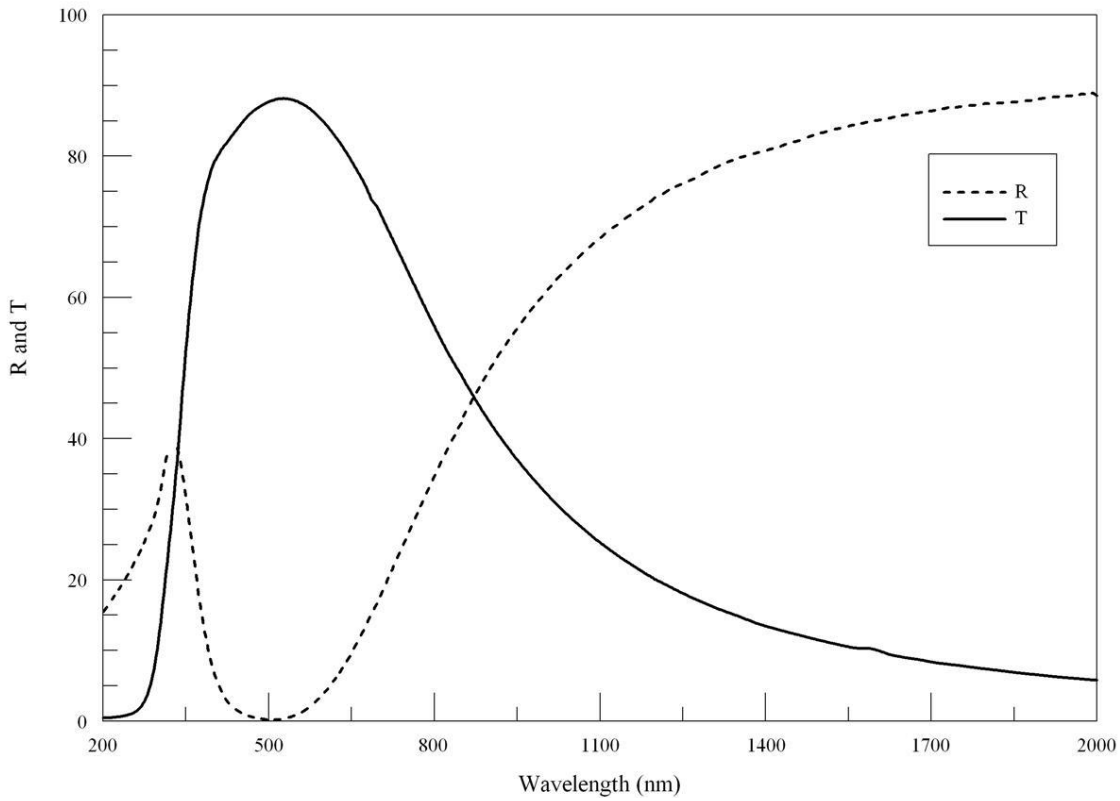

Figure 4.7: Reflectance and transmittance of WO_3/Ag/ WO_3 coatings of thicknesses 35/32/35 (nm). The film was deposited on fused silica substrate.

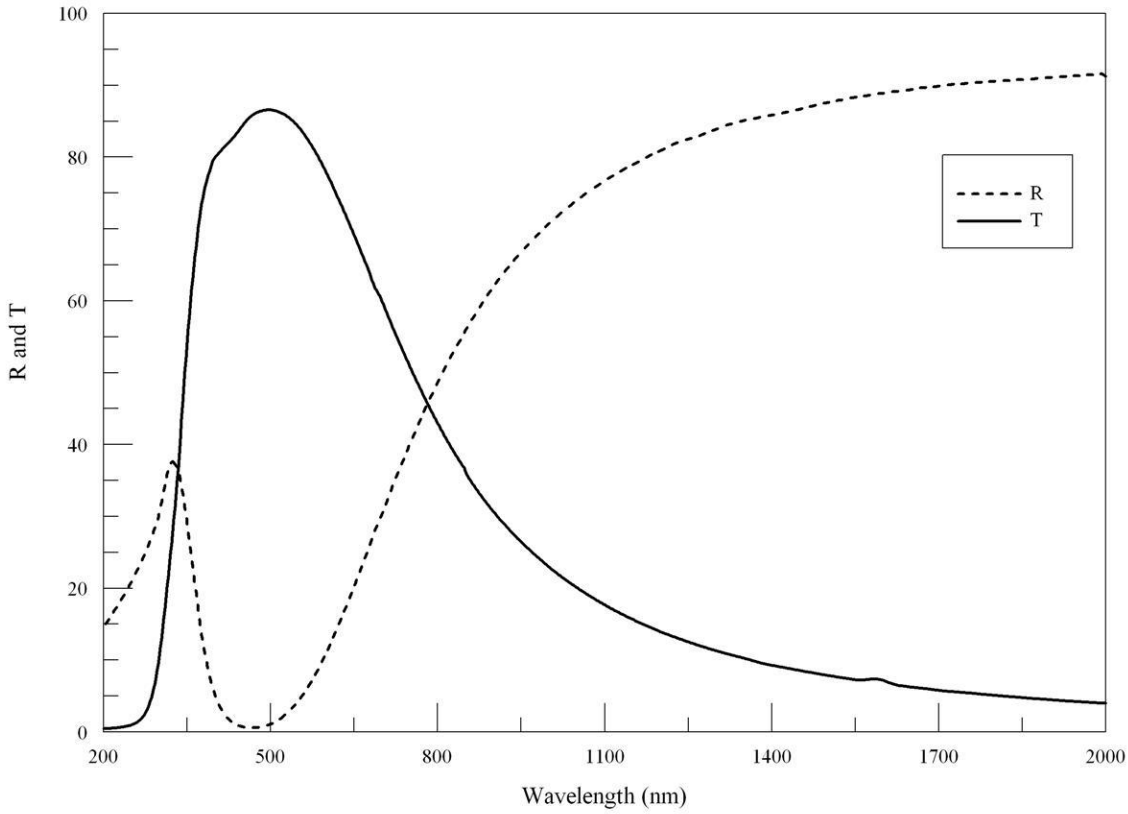

Figure 4.8: Reflectance and transmittance of WO_3/Ag/ WO_3 coatings of thicknesses 35/39/35 (nm). The film was deposited on fused silica substrate.

The transmittance and reflectance of the films were measured after one year, and they showed a change of less than 1%. As a result, the films were durable and did not deteriorate significantly with time.

4.3 Figure of Merit

A figure of merit is used to characterize the performance of the heat mirror films (i.e. determine how much it transmits visible light and reflects infrared heat). T_{VIS} and R_{IR} should be calculated to determine the figure of merit, where T_{VIS} is the average

transmittance of the film in the visible region and R_{IR} is the average reflectance in the infrared region. T_{VIS} and R_{IR} are defined as follows:

$$T_{VIS} = \frac{\int_{400}^{760} T(\lambda)\ [D(\lambda)V(\lambda)]\ d\lambda}{\int_{400}^{760} [D(\lambda)V(\lambda)]\ d\lambda} \tag{5.1}$$

$$R_{IR} = \frac{\int_{760}^{2000} R(\lambda)\ d\lambda}{\int_{760}^{2000}\ d\lambda} \tag{5.2}$$

where $T(\lambda), R(\lambda)$, $D(\lambda)$ and $V(\lambda)$ are the spectral transmittance, spectral reflectance, spectral distribution of sunlight and the spectral sensitivity of the human eye, respectively. The denominator insures normalization. The distribution of $D(\lambda) \times V(\lambda)$ is taken from (ref. [29]) and is shown in Figure 4.9.

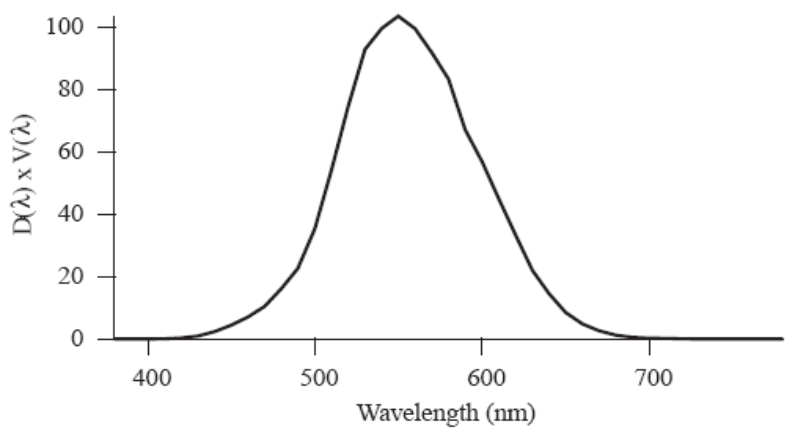

Figure 4.9: Product of the spectral distribution of sunlight, $D(\lambda)$ and the spectral sensitivity distribution of the human eye, $V(\lambda)$used in Japanese industrial standards. [29]

An ideal heat mirror has $T_{VIS} = 1$ and $R_{IR} = 1$. This cannot be achieved practically because, when the thickness of the metal increases, T_{VIS} decreases while R_{IR} increases, and vice versa. Therefore T_{VIS} and R_{IR} may be gathered in one figure of merit F which may be defined as: [26]

$$F = T_{VIS} \cdot R_{IR} \tag{5.3}$$

The functions T_{VIS}, R_{IR} and F are plotted versus thickness of the silver layer for WO_3/Ag and WO_3/Ag/WO_3 and are shown in Figures 4.10-4.12.

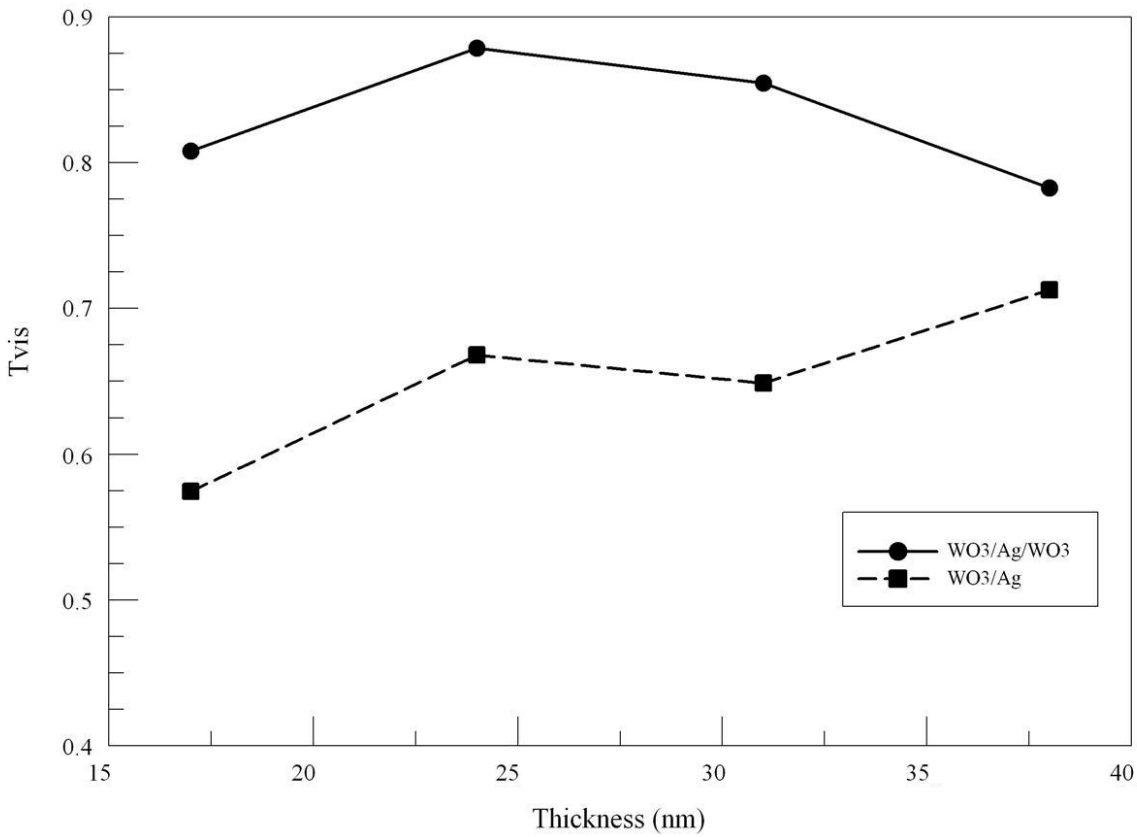

Figure 4.10: T_{VIS} of two-layer WO_3/Ag and three-layer WO_3/Ag/WO_3 coatings for different thicknesses of the silver layer. The thickness of the WO_3 layer is 35 nm.

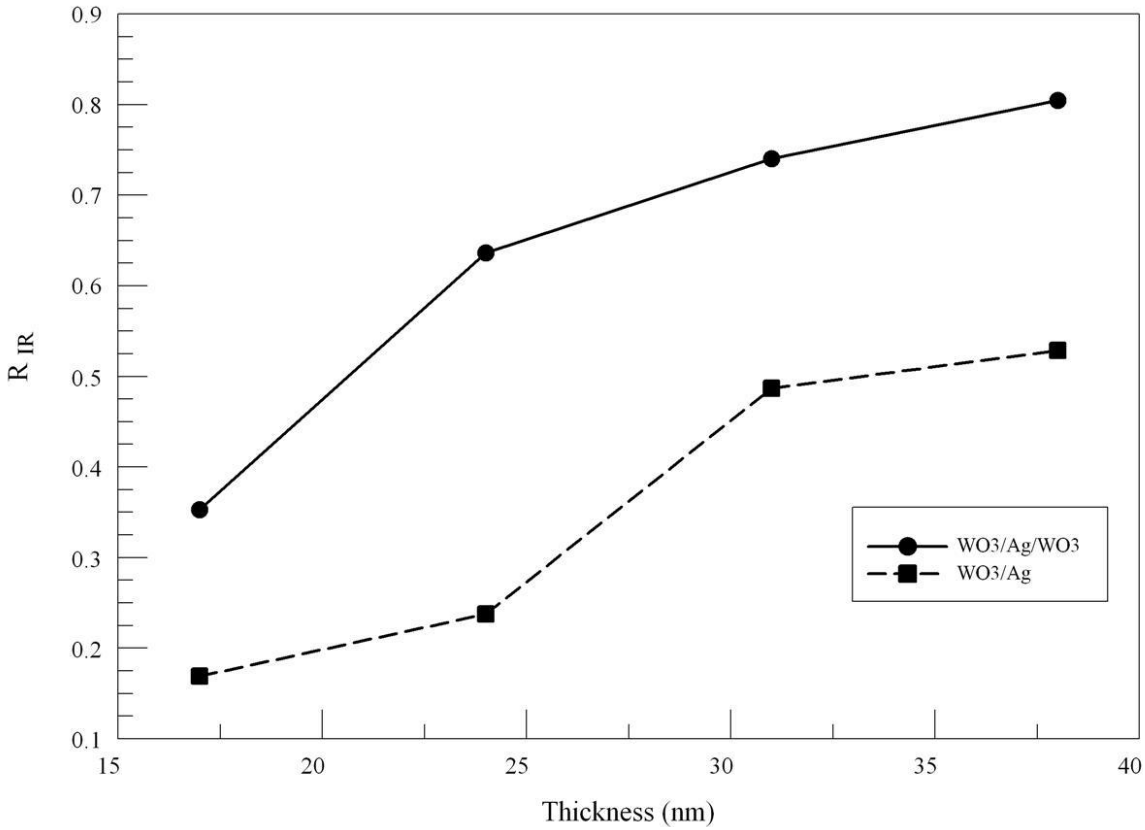

Figure 4.11: R_{IR} of two-layer WO_3/Ag and three-layer WO_3/Ag/WO_3 coatings for different thicknesses of the silver layer. The thickness of the WO_3 layer is 35 nm.

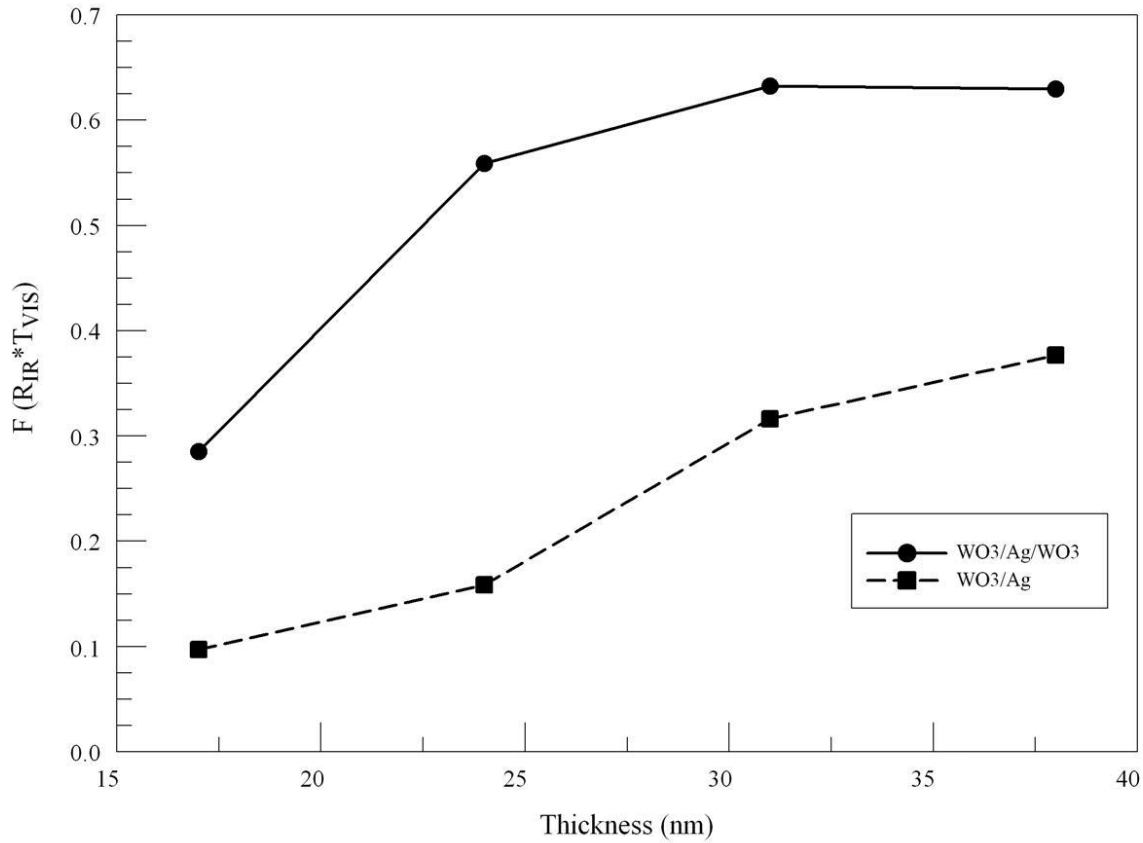

Figure 4.12: Figure of merit *F* of two-layer WO_3/Ag and three-layer WO_3/Ag/WO_3 coatings for different thicknesses of the silver layer. The thickness of the WO_3 layer is 35 nm.

In the case of three-layer WO_3/Ag/WO_3 coatings, the best visible transmittance T_{VIS} occurred at a thickness of 35/25/35 nm while the maximum T_{VIS} for two-layer WO_3/Ag occurred at a thickness of 35/39 nm. In both two and three layers, the infrared reflectance R_{IR} kept rising as the thickness of the silver layer increased, and this is reasonable since the metal layer is responsible for infrared reflectance. Likewise, the figure of merit *F* of the two-layer, shown in Figure 4.12, kept growing with increasing Ag layer thickness. However, for three-layer WO_3/Ag/WO_3 coatings when the thickness

of Ag layer is increased more, the figure of merit *F* reached the maximum value at an optimum Ag thickness of around 32 nm. After that, *F* started gradually decreasing because thicker metal layers destroy visible transmittance.

Chapter 5: GOLD-BASED MULTILAYER COATINGS

In this chapter, the transmittance and reflectance of the multilayer coatings WO_3/Au/WO_3 and WO_3/Au are presented. The thickness of the WO_3 layer was 35 nm, while the thicknesses of the Au layer were 20, 28, 36 and 44 nm.

5.1 Reflectance and Transmittance of Two-Layer (WO_3/Au) Coatings

The transmittance and reflectance spectra of two-layer WO_3/Au coatings are shown in Figures 5.1-5.4 for different values of the thickness of the gold layer. These films did not show the desired properties of a transparent heat mirror, namely high visible transmittance along with high IR reflectance.

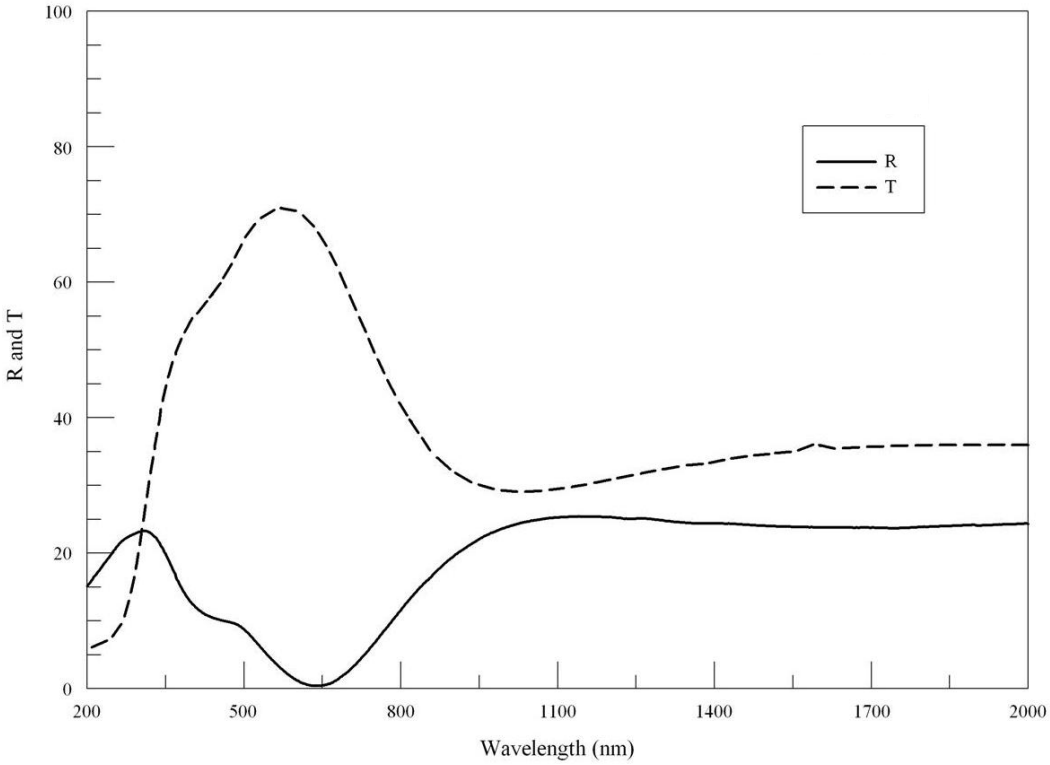

Figure 5.1: Reflectance and transmittance of WO_3/Au coatings of thicknesses 35/20 (nm). The film was deposited on fused silica substrate.

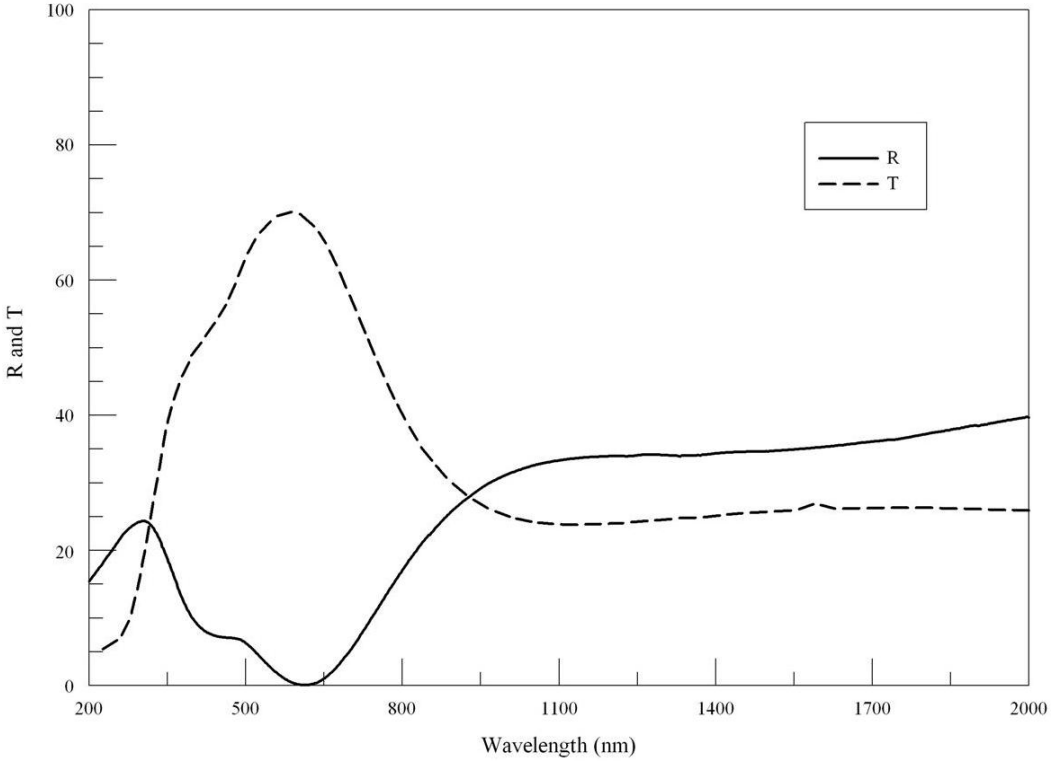

Figure 5.2: Reflectance and transmittance of WO_3/Au coatings of thicknesses 35/28 (nm). The film was deposited on fused silica substrate.

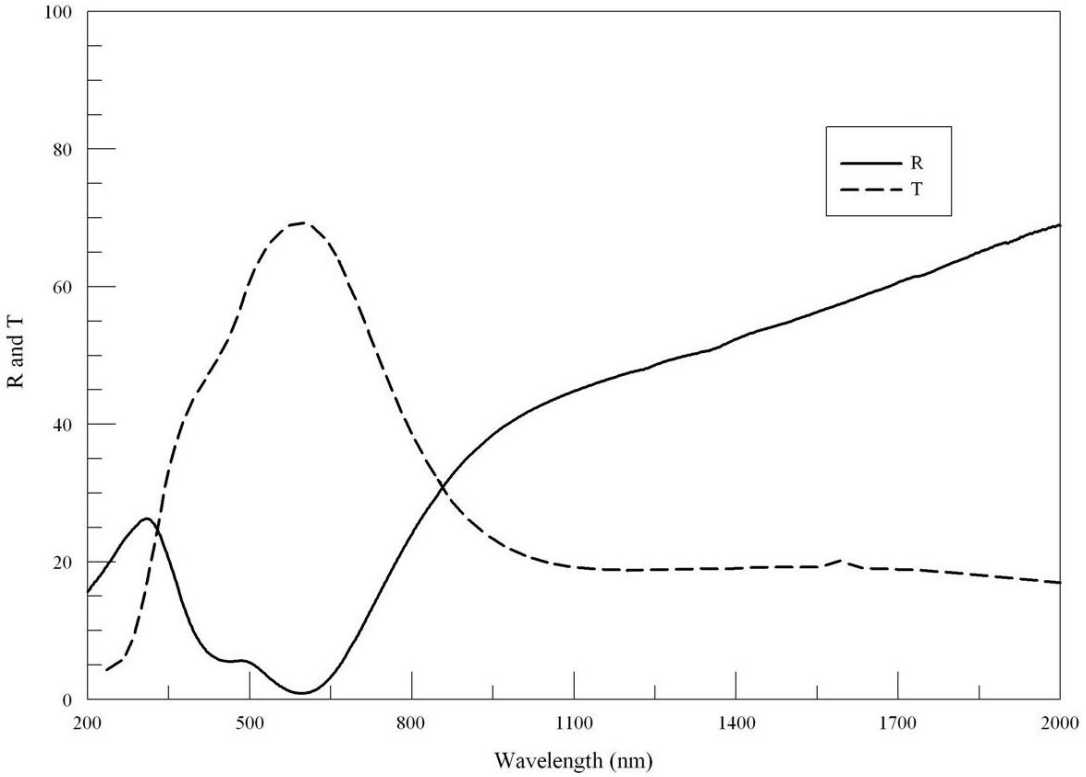

Figure 5.3: Reflectance and transmittance of WO_3/Au coatings of thicknesses 35/36 (nm). The film was deposited on fused silica substrate.

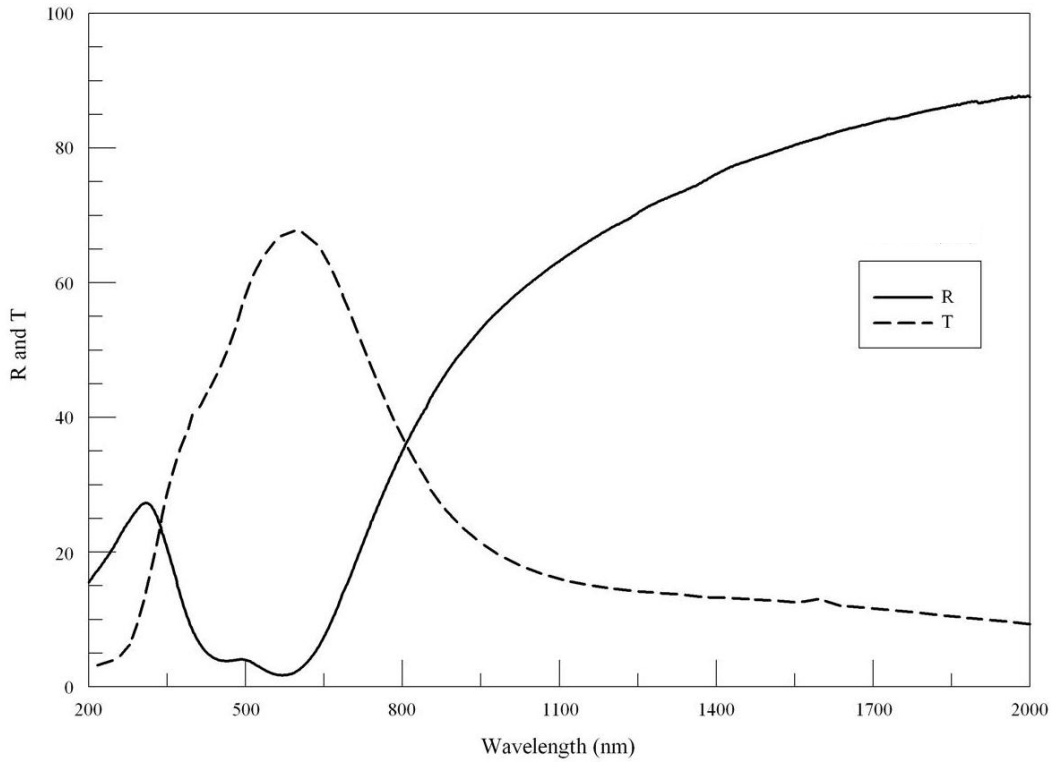

Figure 5.4: Reflectance and transmittance of WO_3/Au coatings of thicknesses 35/44 (nm). The film was deposited on fused silica substrate.

5.2 Reflectance and Transmittance of Three-Layer (WO_3/Au/WO_3) Coatings

The transmittance and reflectance spectra of three-layer WO_3/Au/WO_3 coatings are shown in Figures 5.5-5.8 for different values of the thickness of the gold layer. A heat mirror with a very thin gold layer (Figure 5.5) did not exhibit the required selectivity. Selectivity was improved as the thickness of the gold layer increased. For thicker films (28 nm), the following observations can be made:

(i) The band width of the transmittance narrowed as the thickness of the gold layer increased. This band width was wider than that of WO_3/Ag/WO_3 coatings [6].

(ii) The maximum transmittance decreased as the thickness of the gold layer increased.

(iii) The infrared reflectance increased as the thickness of the gold layer increased.

These observations are consistent with the results on WO_3/Ag/WO_3 coatings shown in Section 4.3. The maximum transmittance was 83.9%, at λ = 674 nm and it was obtained for the heat mirror with a gold layer thickness of 28 nm.

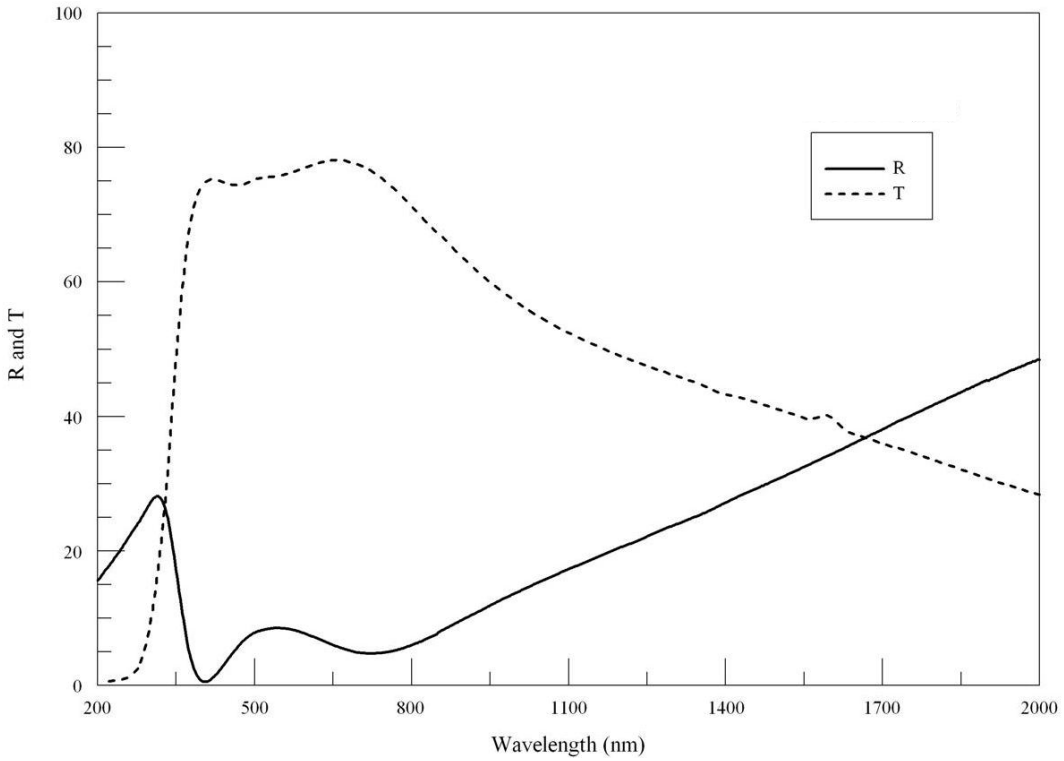

Figure 5.5: Reflectance and transmittance of WO_3/Au/ WO_3 coatings of thicknesses 35/20/35 (nm). The film was deposited on fused silica substrate.

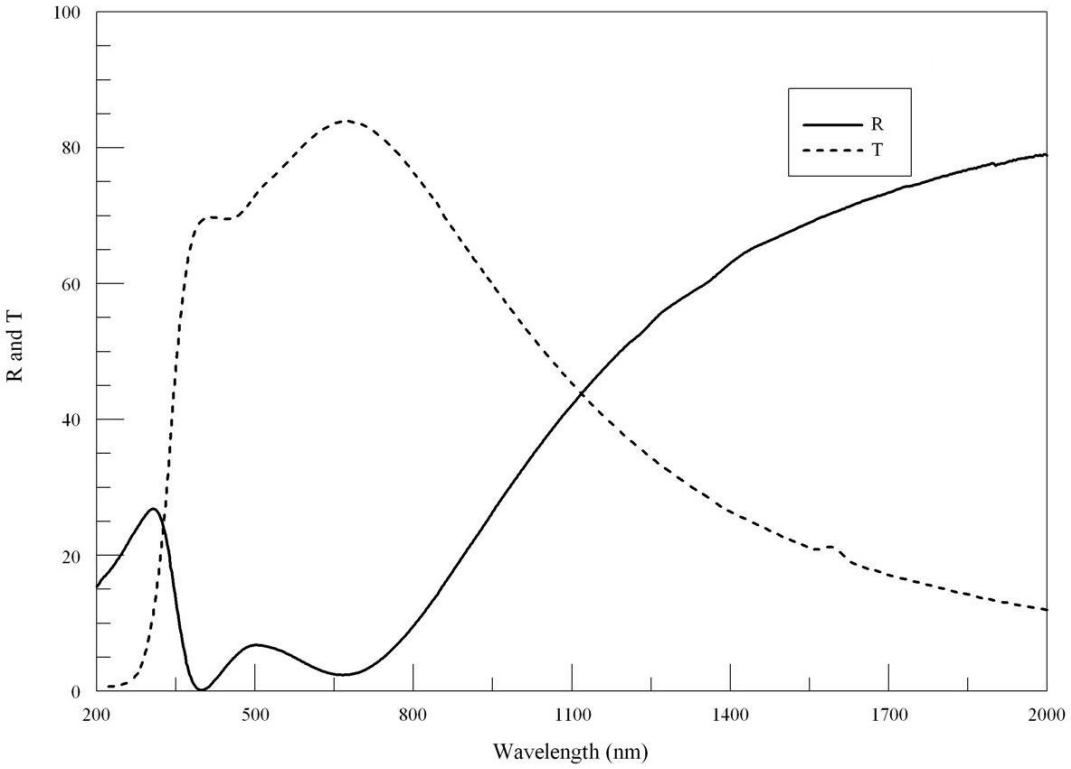

Figure 5.6: Reflectance and transmittance of WO_3/Au/ WO_3 coatings of thicknesses 35/28/35 (nm). The film was deposited on fused silica substrate.

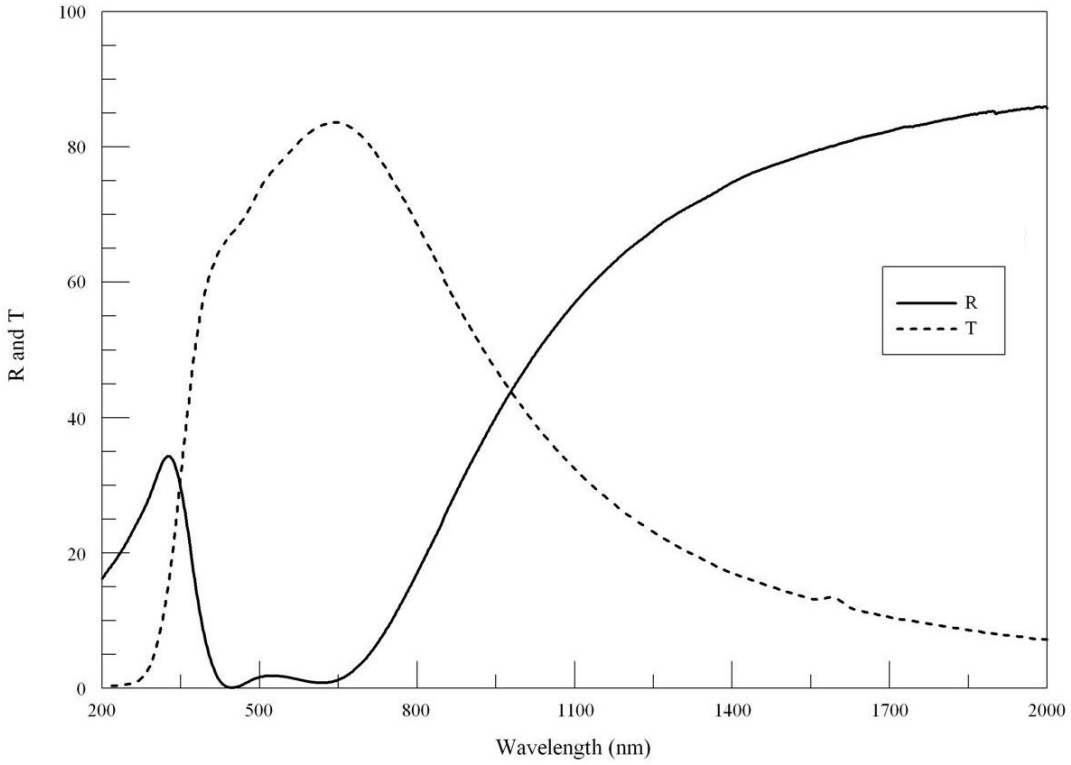

Figure 5.7: Reflectance and transmittance of WO_3/Au/ WO_3 coatings of thicknesses 35/36/35 (nm). The film was deposited on fused silica substrate.

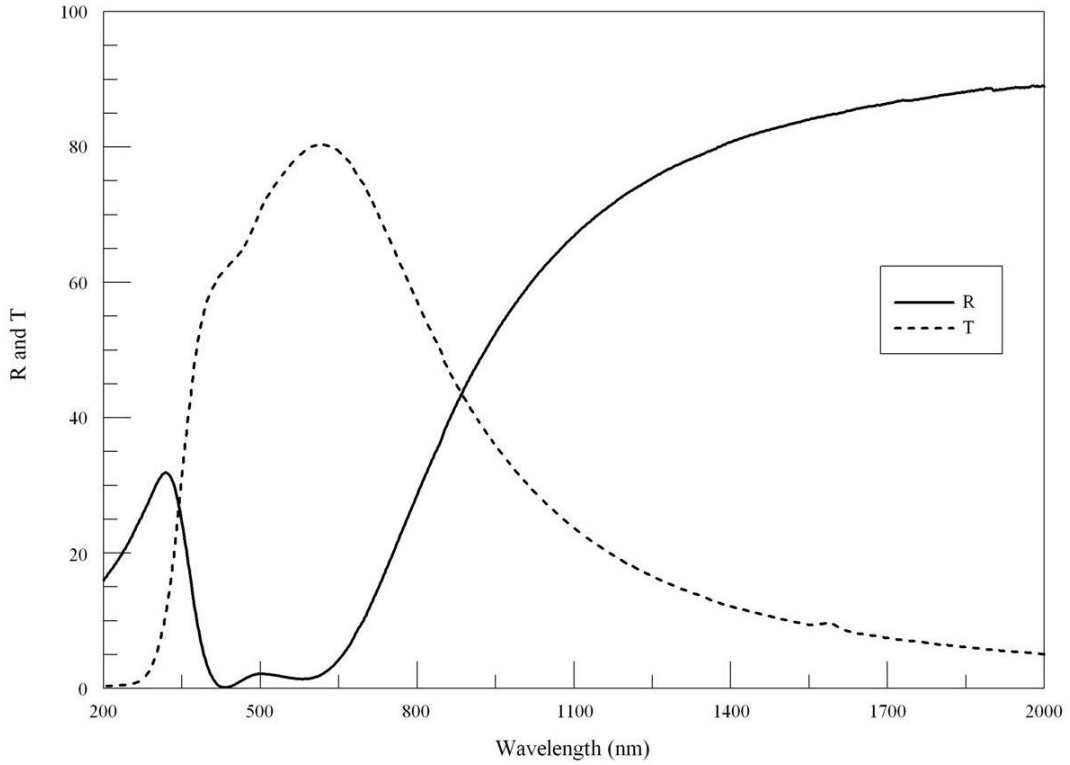

Figure 5.8: Reflectance and transmittance of WO_3/Au/ WO_3 coatings of thicknesses 35/44/35 (nm). The film was deposited on fused silica substrate.

The transmittance and reflectance of the films were measured after one year, and showed a change of less than 1%. As a result, we can say that the films were durable and did not deteriorate significantly with time.

5.3 Figure of Merit

The concept of figure of merit was introduced in section 5.3. Figures 5.9-5.11 show plots of T_{VIS}, R_{IR} and F versus the thickness of the gold layer for multilayers of WO_3/Au and WO_3/Au/WO_3.

It is obvious from Figures 5.9 and 5.10 that the visible transmittance and IR reflectance of WO_3/Au/WO_3 were better than those of WO_3/Au. In the case of WO_3/Au/WO_3, the best visible transmittance T_{VIS} occurred at a thickness of 35/36/35 nm while the T_{VIS} of WO_3/Ag decreased as the thickness of the gold layer increased. In both two- and three-layer coatings, the values of infrared reflectance R_{IR} kept rising, and they approached each other as the thickness of the gold layer increased. This implies that the metal layer was the main cause for reflecting the infrared radiation.

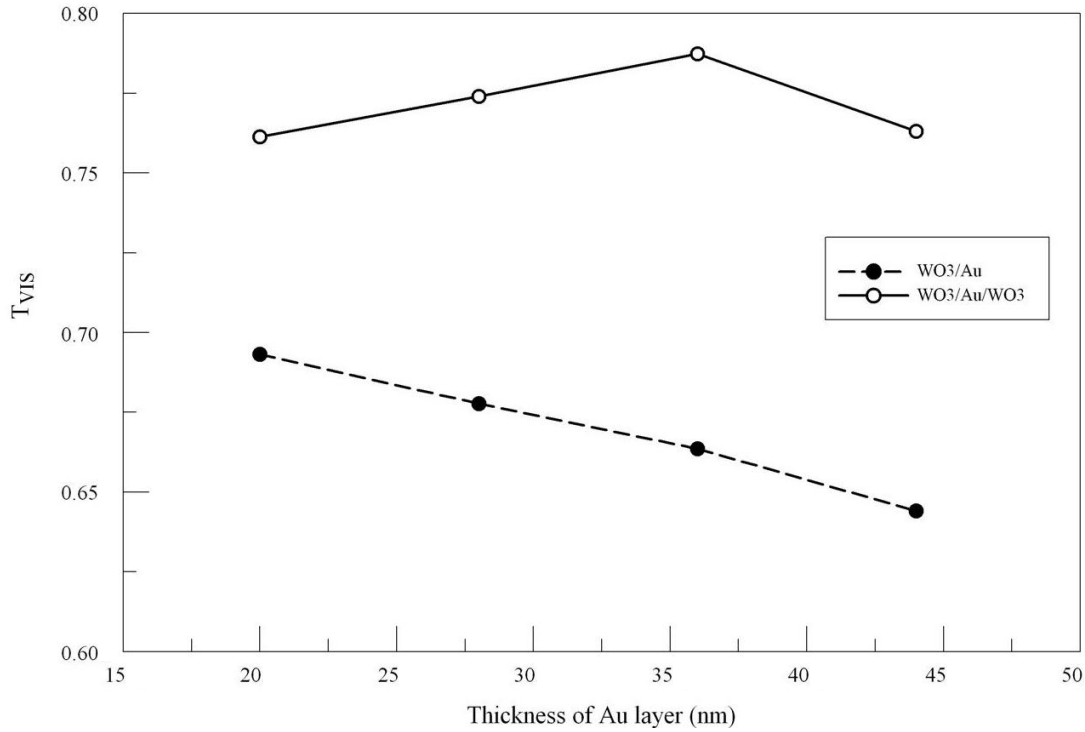

Figure 5.9: T_{VIS} of two-layer WO_3/Au and three-layer WO_3/Au/WO_3 coatings for different thickness of the gold layer. The thickness of WO_3 layer is 35 nm.

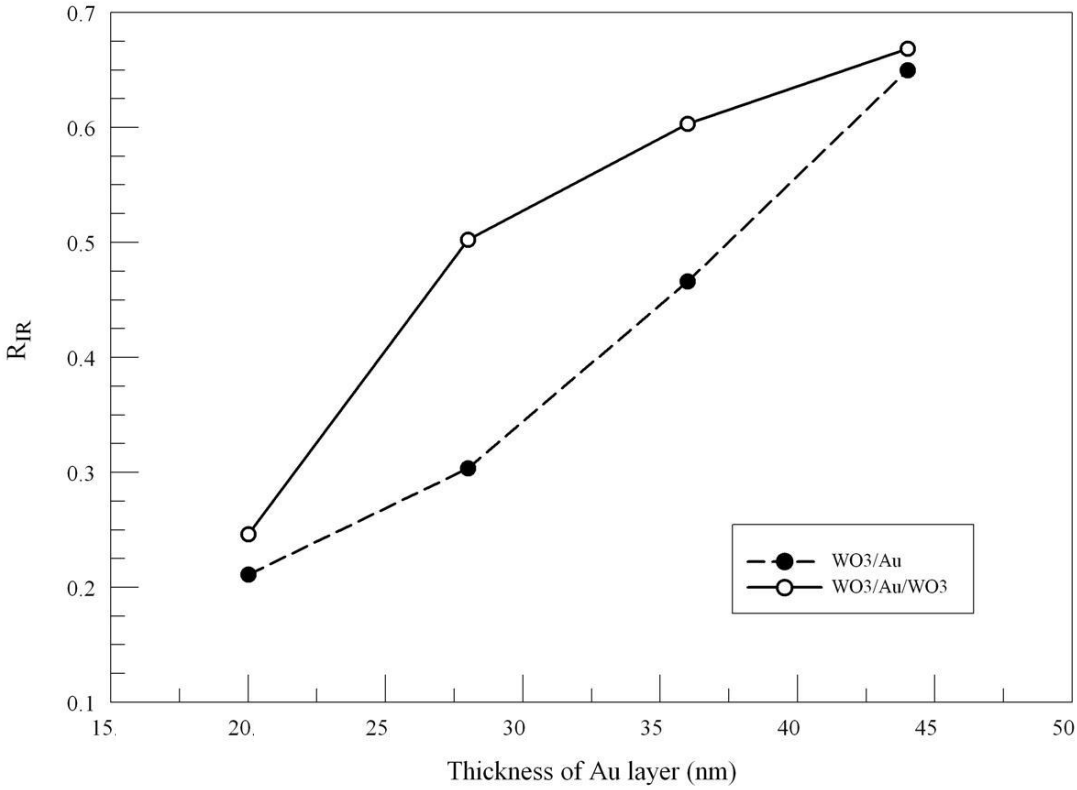

Figure 5.10: R_{IR} of two-layer WO_3/Au and three-layer WO_3/Au/WO_3 coatings for different thickness of the gold layer. The thickness of WO_3 layer is 35 nm.

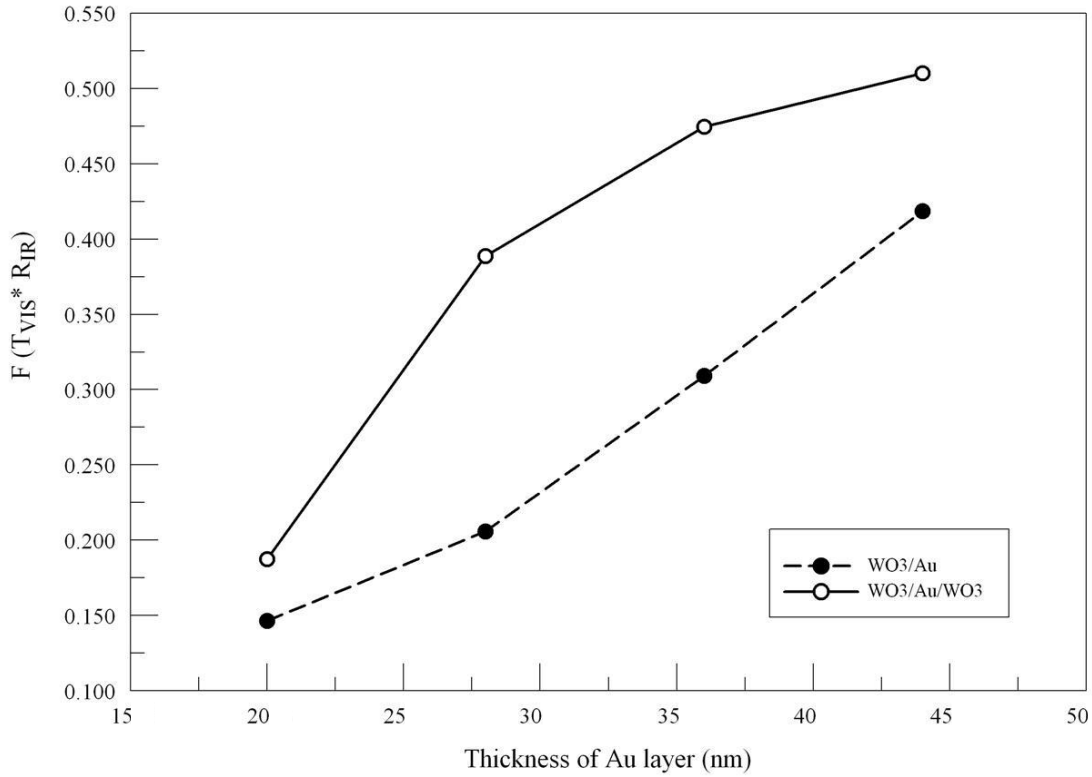

Figure 5.11: Figure of merit *F* of two-layer WO_3/Au and three-layer WO_3/Au/WO_3 for different thickness of the gold layer. The thickness of WO_3 layer is 35 nm.

5.4 Comparing the Performance of (WO_3/Ag), (WO_3/Au), (WO_3/Ag/WO_3) and (WO_3/Ag/WO_3) Coatings

Now, a question may arise. Which coating is better? Two or three layers, silver-based or gold-based multilayers? This question can be answered by looking at the figures of merit. Then, depending on the applications, the decision can be made. For example, if visible transparency of the film has high priority in the application, the evaluation should be based mainly on T_{VIS} measurements, while if reflecting heat is more important in the application, then R_{IR} measurements should be heavily considered. However, some applications need good performance in both IR reflectance and visible transmittance. In that case, the figure of merit $F\ (= T_{VIS} \cdot R_{IR})$ is used in the evaluation. Figure 5.12 shows the figure of merit F of the (WO_3/Ag), (WO_3/Ag/WO_3), (WO_3/Au) and (WO_3/Au/WO_3) coatings. Using T_{VIS}, R_{IR} and F measurements, the following observations can be made:

(i) The three-layer (WO3/Ag/WO_3 and WO_3/Au/WO_3) coatings were better than two-layer (WO_3/Ag and WO_3/Au) coatings.

(ii) The IR reflectance R_{IR} for all coatings increased as the thickness of the metal layer increased.

(iii) Regarding the two-layer coatings, the performance of the WO_3/Ag coatings was comparable to the WO_3/Au coatings, where the values of *F* were close as shown in Figure 5.12.

(iv) The $WO_3/Ag/WO_3$ coating showed the best performance transparent heat mirrors when the thickness of the silver was 32 nm.

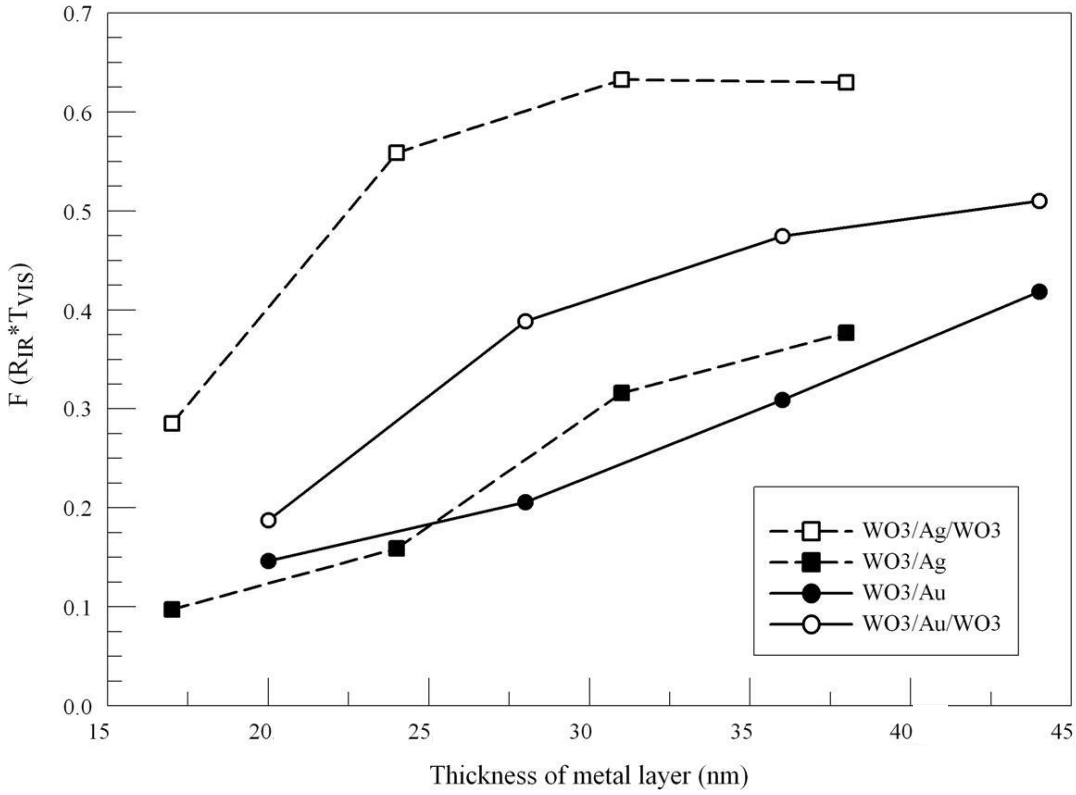

Figure 5.12: Figure of merit *F* of WO_3/Ag, $WO_3/Ag/WO_3$, WO_3/Au and $WO_3/Au/WO_3$.

5.5 XPS Depth Profiles of (WO_3/Ag/WO_3) and (WO_3/Au/WO_3)

The major factor affecting the stability of a heat mirror is the diffusion of the metal atoms across the dielectric layers [30]. Also, depositing a dielectric layer on top of the metal layer damages the surface of the metal to some extent [31]. This induces instability in the metal layer and subsequent dissociation of metal atoms from the metallic layer [31]. The diffusion process reduces the effective thickness of the metal layer [32]. The selectivity of heat mirrors depends on the sharpness of the layers' interfaces, which is degraded by inter-diffusion [15]. Figures 5.13 and 5.14 show the XPS depth profiles of WO3/Ag/WO_3 and WO_3/Au/WO_3. The profiles were calculated from the areas of the W 4f, O 1s, Ag 3d, and Au 4f peaks, taking into account the atomic sensitivity factor of each peak. It is obvious from the XPS depth profiles that the interfaces between the layers were not sharp. This may indicate the occurrence of inter-diffusion between the tungsten oxide and the metal layers. The atomic concentration of oxygen is almost double the concentration of tungsten. This indicates that the dielectric layers were WO_2 although the starting dielectric material was WO_3.

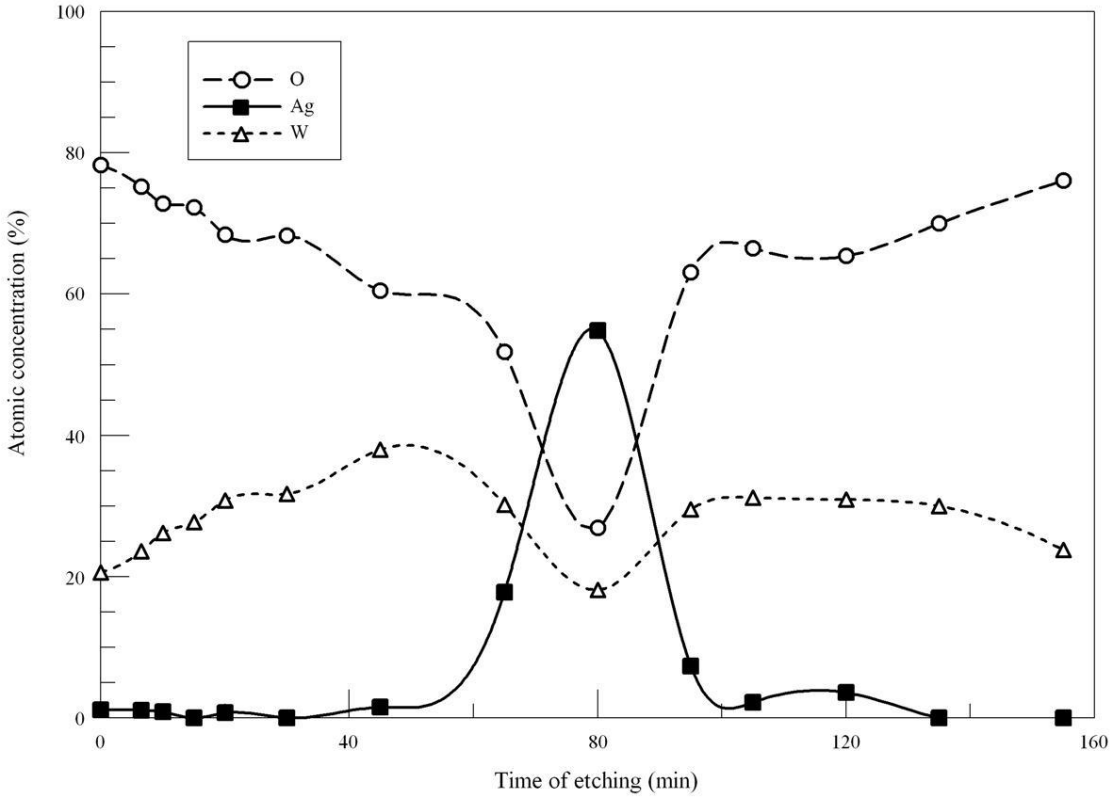

Figure 5.13: XPS depth profile spectra of WO_3/Ag/WO_3 of thickness 35/25/35 nm done 6 months after the deposition. It shows a diffusion of silver in the WO_3 layers.

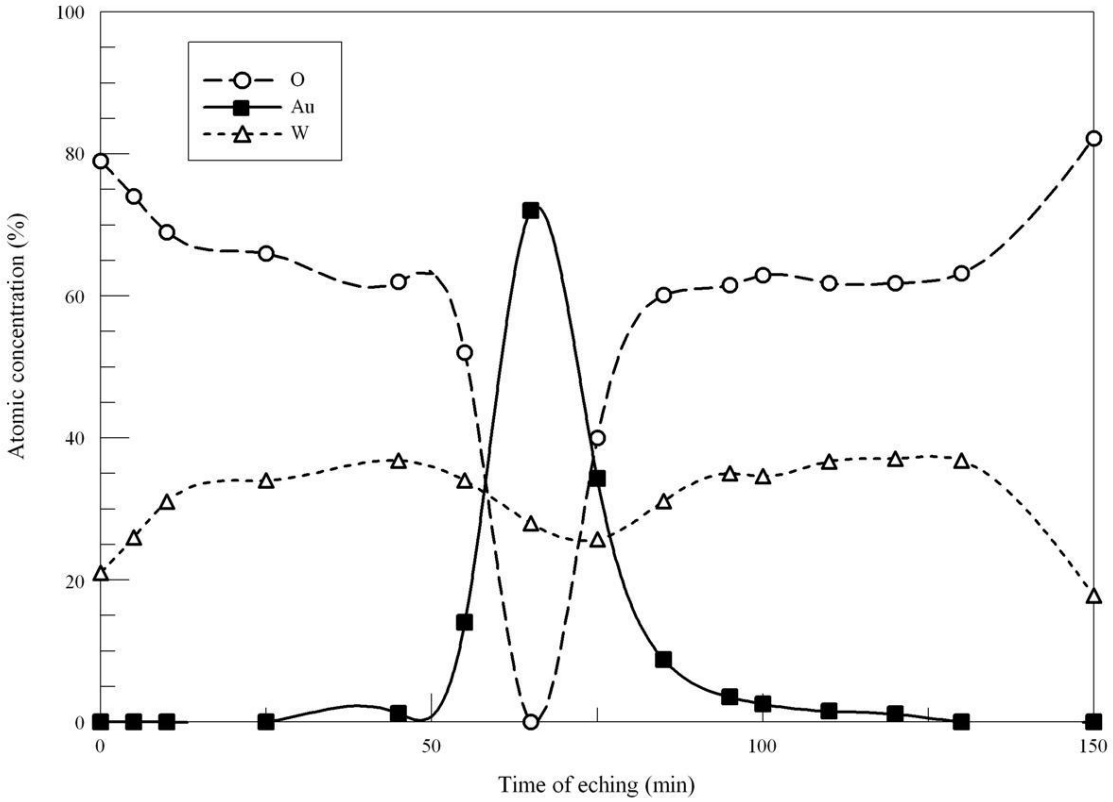

Figure 5.14: XPS depth profiles of WO_3/Au/WO_3 of thickness 35/28/35 nm done 6 months after the deposition. It shows a relatively smaller diffusion of gold in the WO_3 layers.

Chapter 6: Conclusion

Transparent heat mirrors based on WO_3/Ag, WO_3/Au, WO_3/Ag/WO_3, and WO_3/Au/WO_3 multilayers were fabricated by using thermal evaporation. The effect of the layer thickness of the metals (Ag and Au) and dielectric (WO_3) on the optical spectra was investigated. Suitable transparent heat mirrors were obtained for WO_3 with a thickness of 35 nm. The three-layer coatings (WO3/Ag/WO_3 and WO_3/Au/WO_3) exhibited better transparent heat mirror performance than two-layer coatings (WO_3/Ag and WO_3/Au). The performance of the WO_3/Ag coatings was comparable to the WO_3/Au coatings. For all coatings, the infrared reflectance increased as the thickness of the metal layer increased. The WO_3/Ag/WO_3 coatings showed the best performance transparent heat mirrors. These coatings exhibited excellent visible transmittance, with a maximum around 88.3% at 554 nm. For 35-nm-thick tungsten oxide layers, the optimum thicknesses of the silver layer and the gold layer were 32 and 44 nm, respectively. The XPS depth profiles showed that the dielectric layers were WO_2.

Suggestion for further work:

- Investigate the WO_3 layers of 45 and 55 nm thicknesses.
- Using other metals such as Al and Cu.
- Investigate five-layer (D/M/D/M/D) coatings.
- Deposit the films by using chemical and sputtering deposition techniques.

Appendix A: Multilayer Films for a WO_3 Thickness of 70 nm

As illustrated in the theory, getting a good transparent heat mirror requires the thickness of the dielectric to be greater than $\lambda/8n_D$, where λ is the wavelength corresponding to minimum reflection, and n_D is the refractive index of the dielectric at that wavelength. The refractive index of WO_3 equals 2.014 at λ =550 nm which is the center visible range. Therefore, the thickness of WO_3 layers must be greater than 34 nm. In this study, two thicknesses of WO_3 were investigated. The first thickness was 35 nm which is the lowest possible thickness. This thickness produced high-quality transparent heat mirrors whose properties were presented in chapters 4 and 5. The second thickness (70 nm) did not produce a suitable heat mirror and its results are presented here for comparison.

A.I Three-layer ($WO_3/Ag/WO_3$)

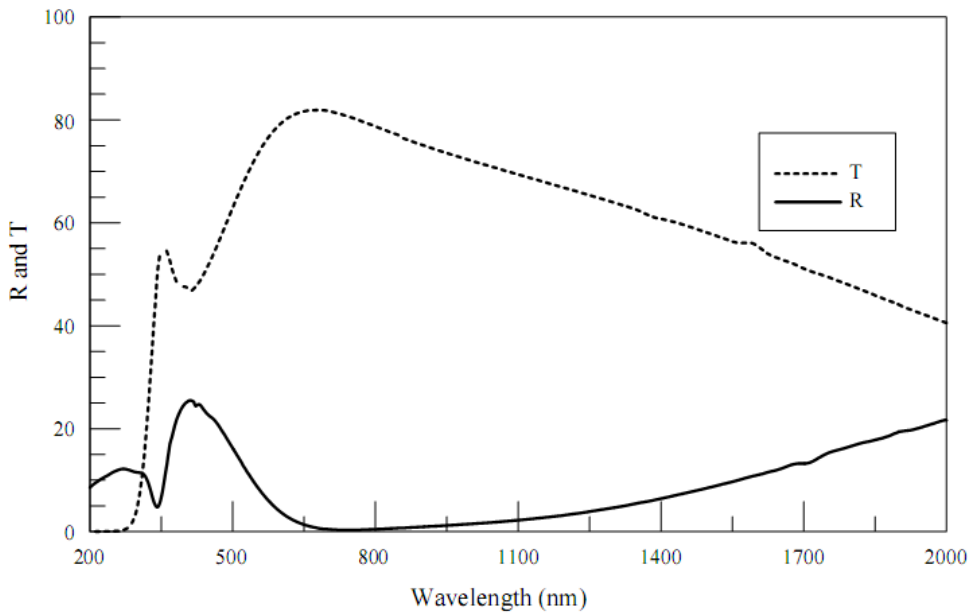

Figure A.1: Reflectance and transmittance of $WO_3/Ag/WO_3$ of thicknesses 70/18/70 (nm). The film was deposited on fused silica substrate.

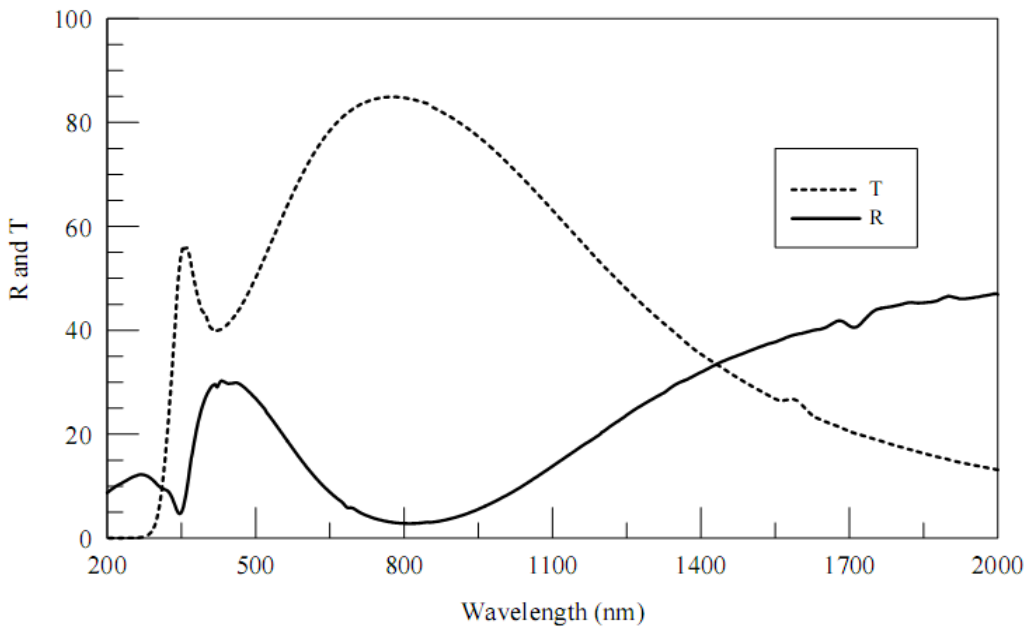

Figure A.2: Reflectance and transmittance of $WO_3/Ag/WO_3$ of thicknesses 70/25/70 (nm). The film was deposited on fused silica substrate.

A.II Two-layer (WO_3/Ag)

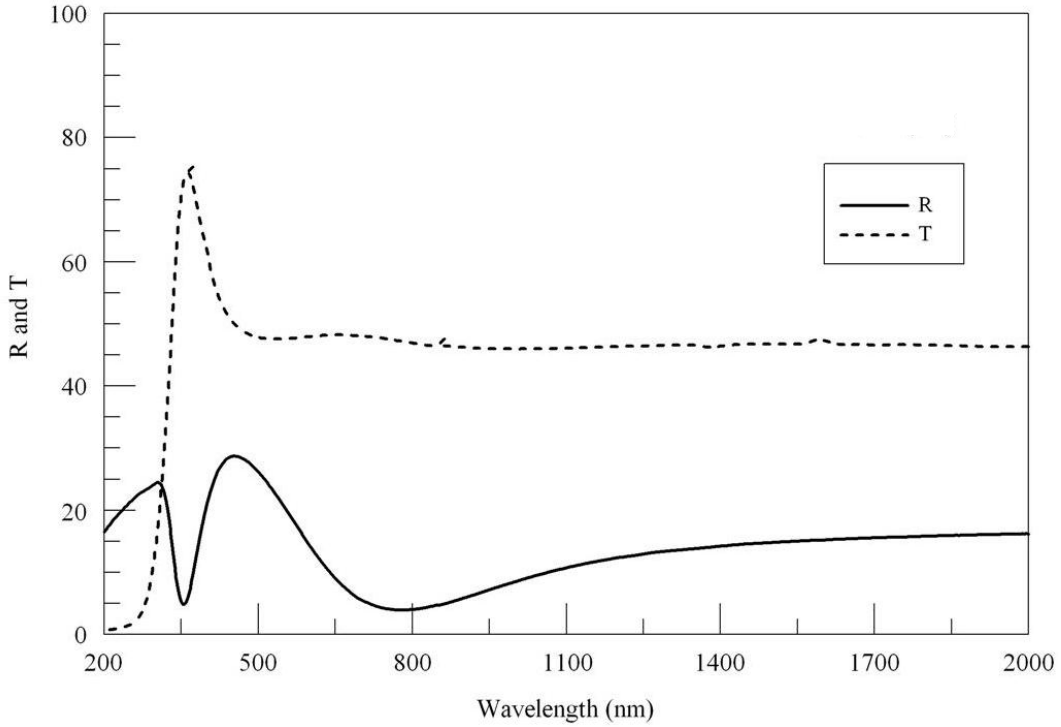

Figure A.3: Reflectance and transmittance of WO3/Ag of thicknesses 70/18 (nm). The film was deposited on fused silica substrate.

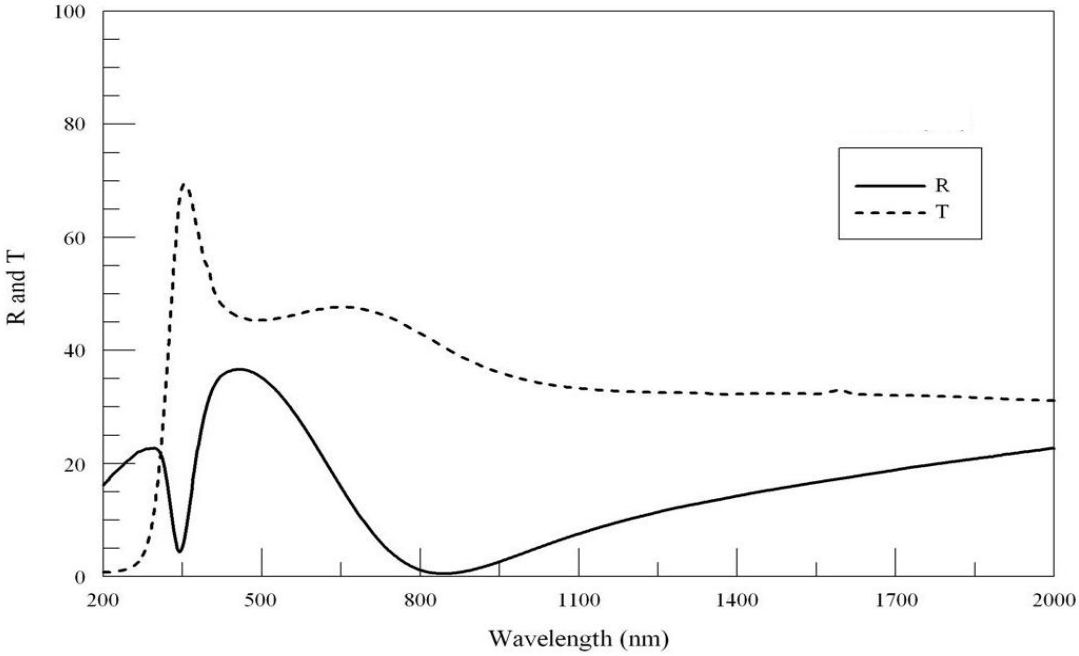

Figure A.4: Reflectance and transmittance of WO_3/Ag of thicknesses 70/25 (nm). The film was deposited on fused silica substrate.

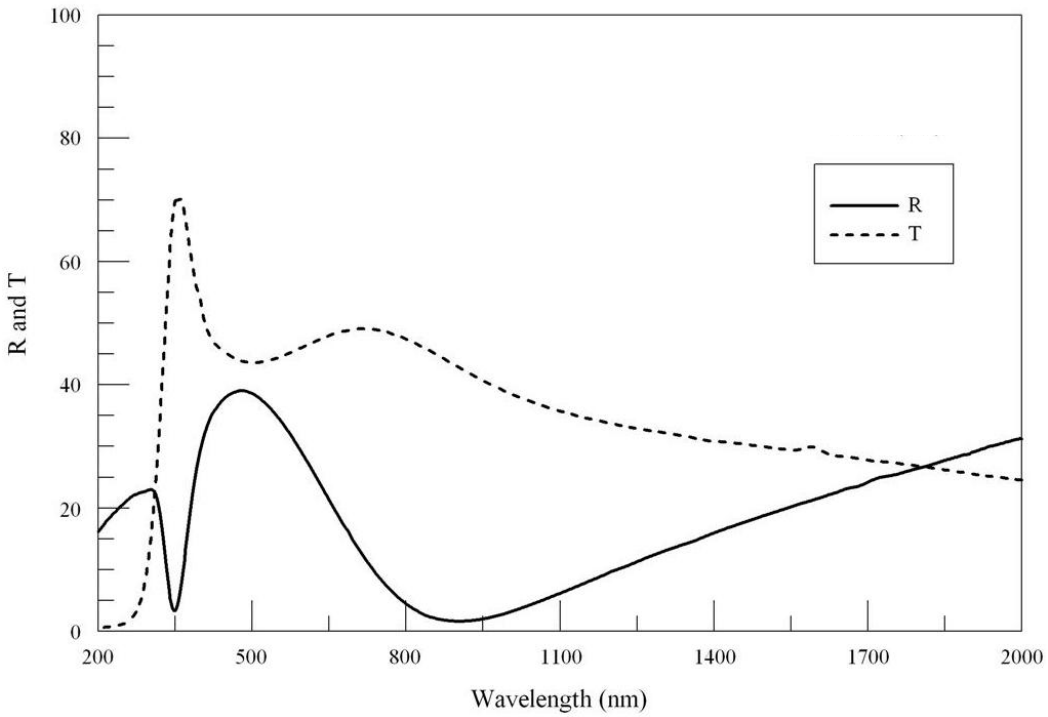

Figure A.5: Reflectance and transmittance of WO_3/Ag of thicknesses 70/32 (nm). The film was deposited on fused silica substrate.

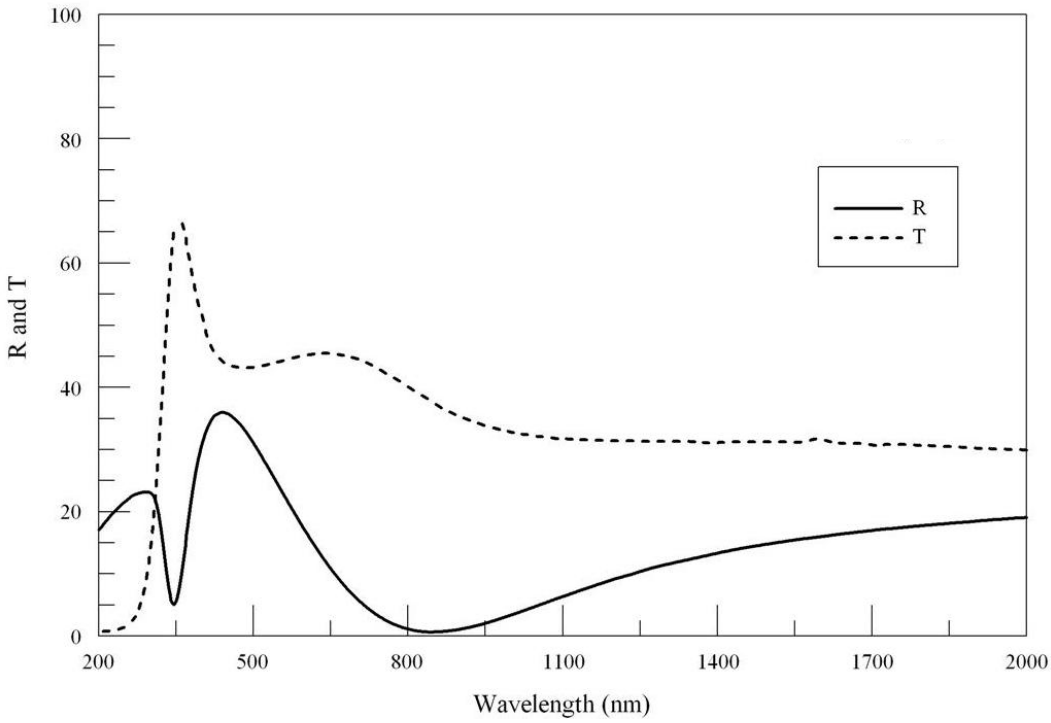

Figure A.6: Reflectance and transmittance of WO_3/Ag of thicknesses 70/39 (nm). The film was deposited on fused silica substrate.

A.III Three-layer ($WO_3/Au/WO_3$)

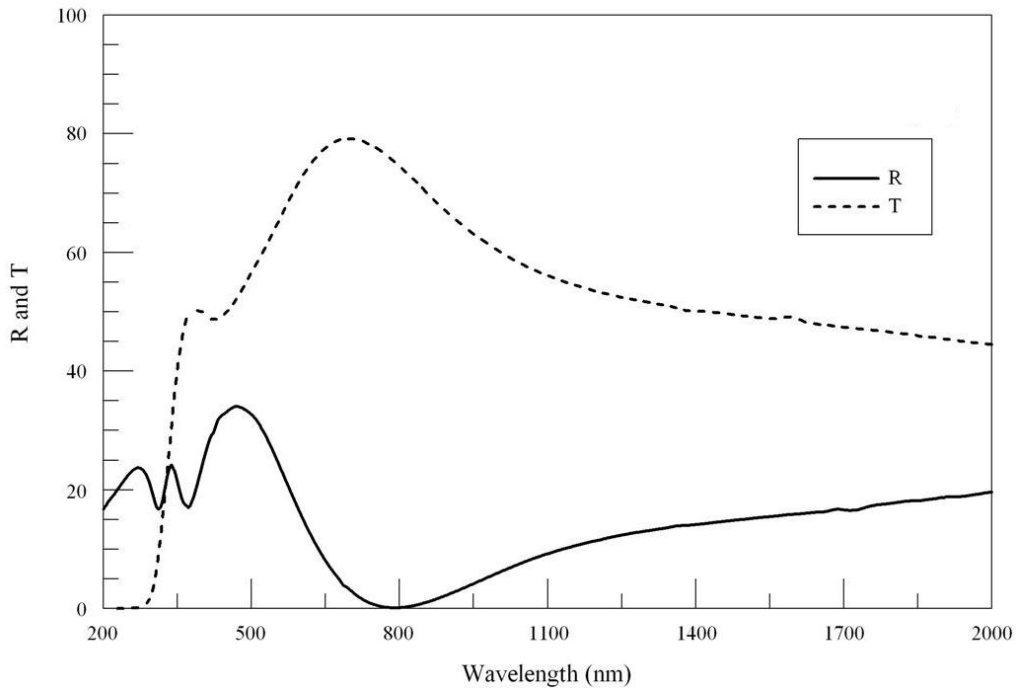

Figure A.7: Reflectance and transmittance of WO3/Au/WO3 of thicknesses 70/20/70 (nm). The film was deposited on fused silica substrate.

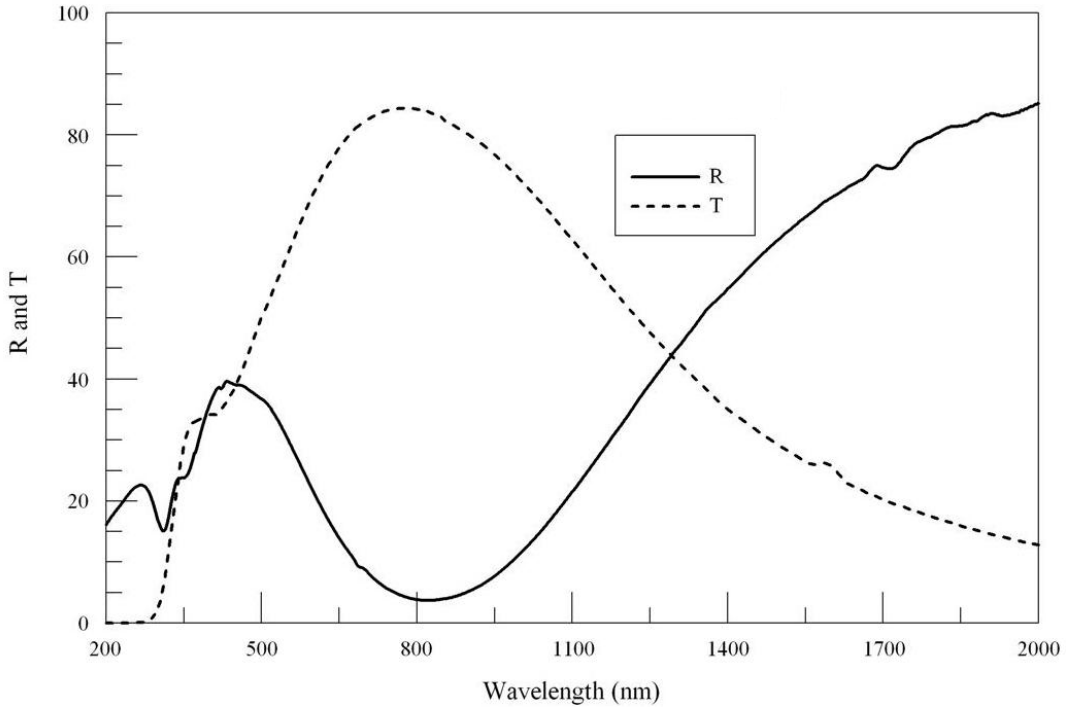

Figure A.8: Reflectance and transmittance of WO_3/Au/WO_3 of thicknesses 70/28/70 (nm). The film was deposited on fused silica substrate.

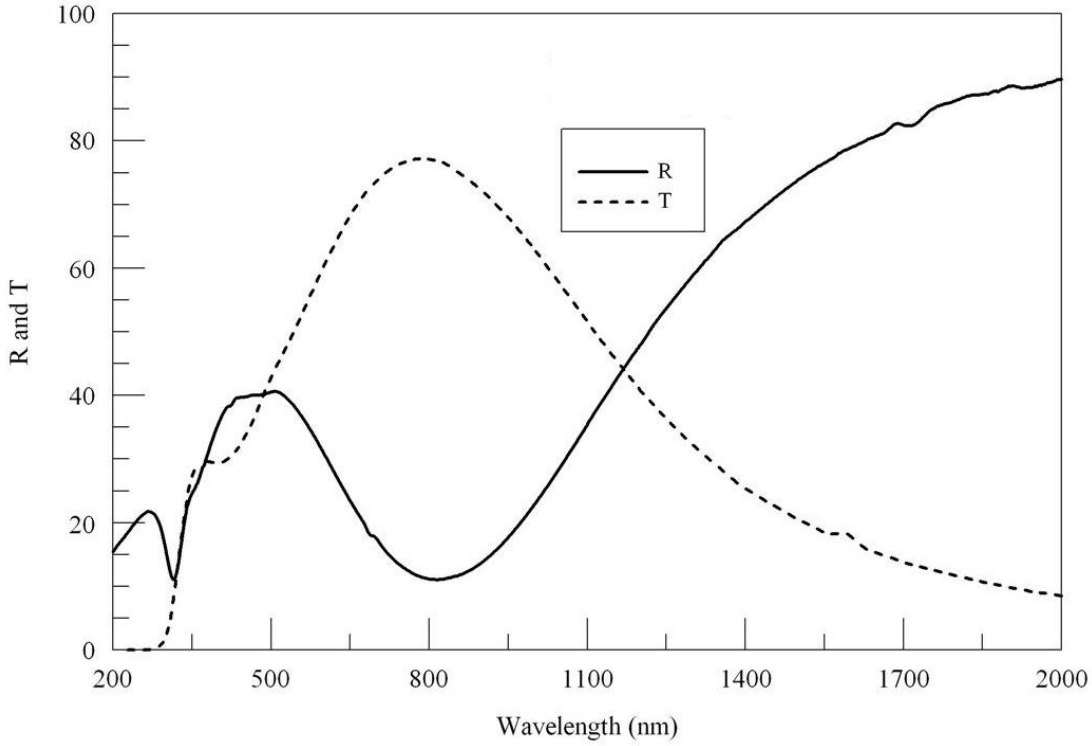

Figure A.9: Reflectance and transmittance of WO3/Au/WO3 of thicknesses 70/36/70 (nm). The film was deposited on fused silica substrate.

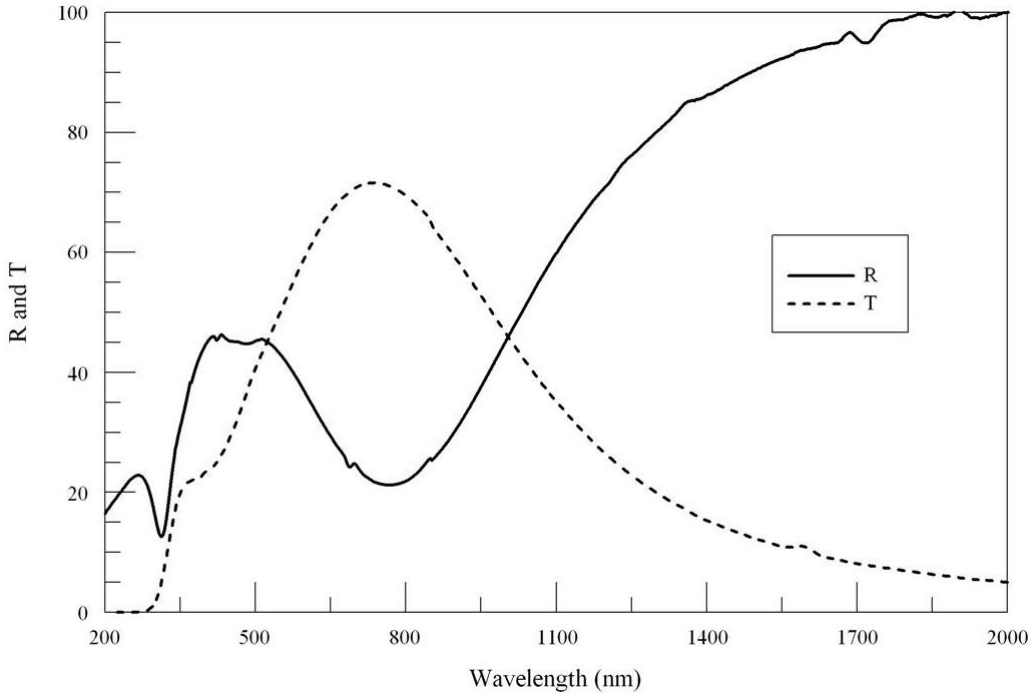

Figure A.10: Reflectance and transmittance of $WO_3/Au/WO_3$ of thicknesses 70/44/70 (nm). The film was deposited on fused silica substrate.

A.IV Two-layer (WO_3/Au)

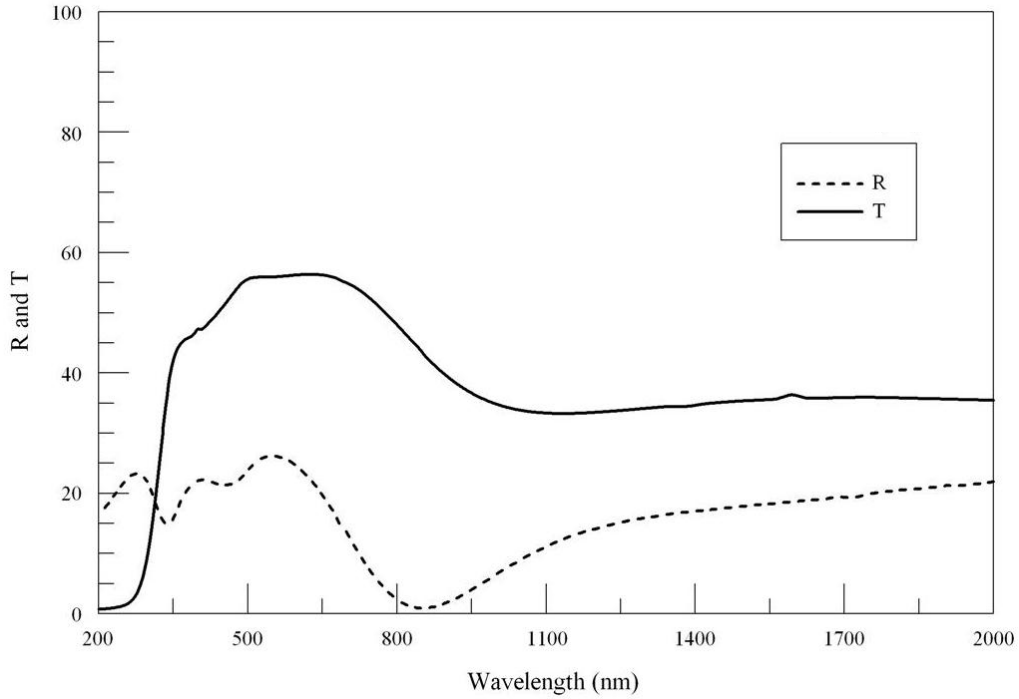

Figure A.11: Reflectance and transmittance of WO_3/Au of thicknesses 70/20 (nm). The film was deposited on fused silica substrate.

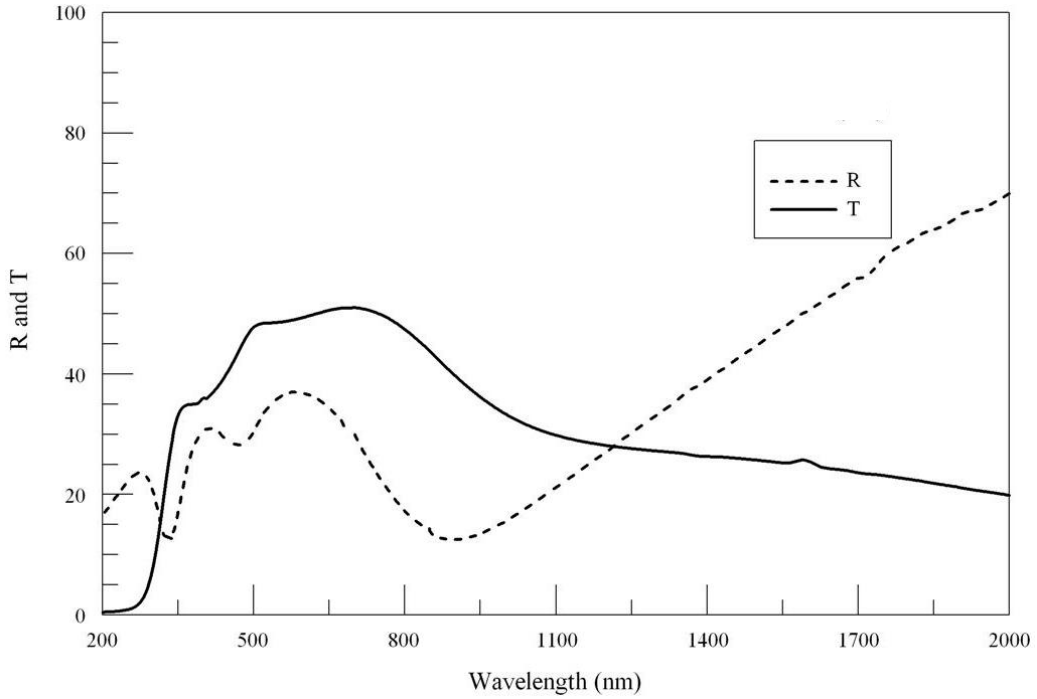

Figure A.12: Reflectance and transmittance of WO_3/Au of thicknesses 70/28 (nm). The film was deposited on fused silica substrate.

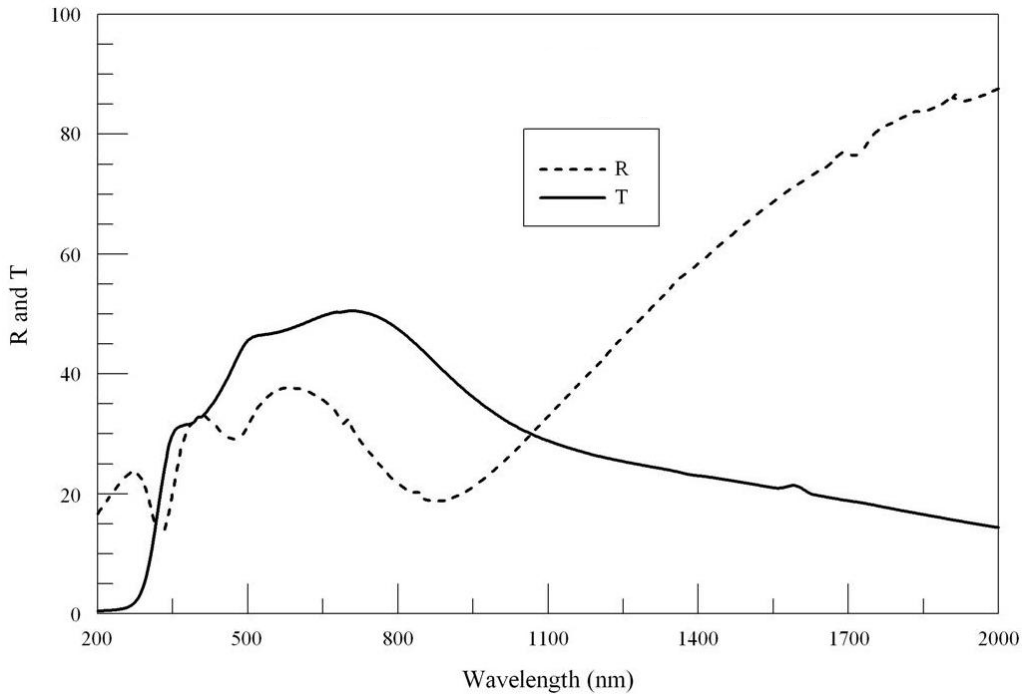

Figure A.13: Reflectance and transmittance of WO_3/Au of thicknesses 70/36 (nm). The film was deposited on fused silica substrate.

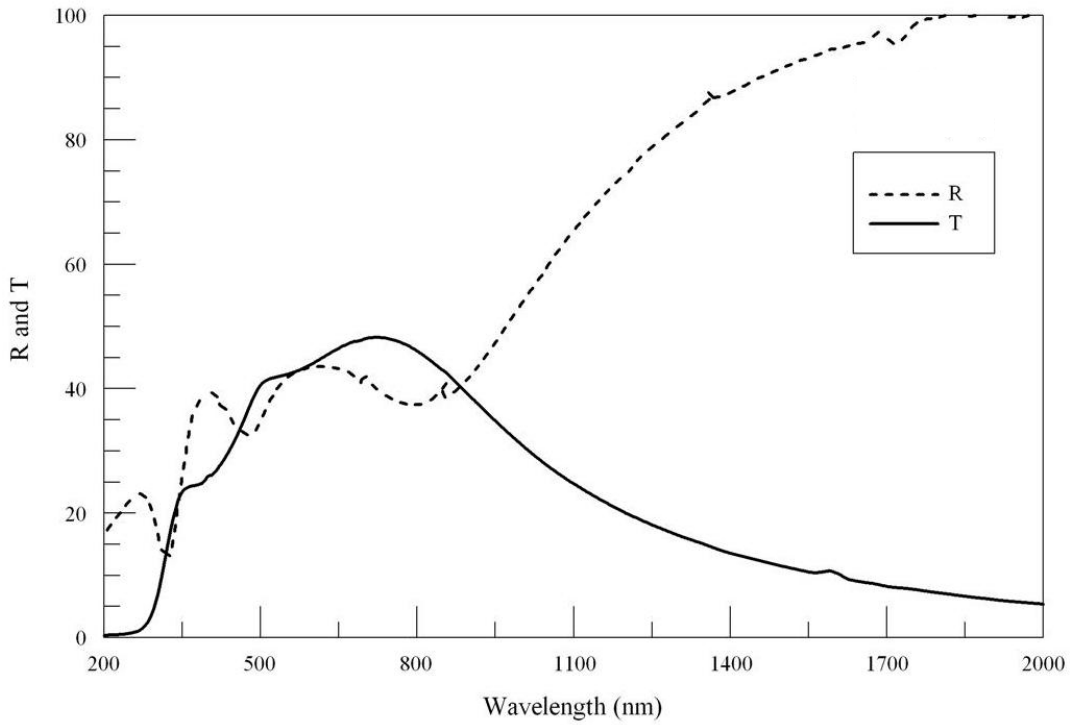

Figure A.14: Reflectance and transmittance of WO_3/Au of thicknesses 70/44 (nm). The film was deposited on fused silica substrate.

References

[1] R. E. Hummel, "*Electornic Properies of Materials".* New York: Springer Verlag (2000).

[2] B. E. A. Saleh, M. C. Teich, "*Fundamentals of Photonics*", John Wiley & Sons, Inc (2001)

[3] F. L. Pedrotti, "*Introduction to Optics",* USA: Prentice Hall PTR (1996).

[4] P. Jin, L. Miao, S. Tanemura, G. Xu, M. Tazawa, K. Yoshimura, "*Formation and characterization of TiO_2 thin films with application to a multifunctional heat mirror"*, Applied Surface Science **212-213** (2003) 775-781.

[5] M. Kojima, F. Takahashi, K. Kinoshita, T. Nishibe, M. Ichidate , "*Transparent furnace made of heat mirror*", Thin Solid Films **392** (2001) 349-354.

[6] B. Karlsson, E. Valkonen, T. Karlsson, and C. G-. Ribbing*, "Materials for solar-transmitting heat-reflecting coatings",* Thin Solid Films **86** (1981) 91-98.

[7] E. Valkonen, B. Karlsson and C-G. Ribbing, "*Solar optical properties of thin films of Cu, Ag, Au, Cr, Fe, Co, Ni and Al"*, Solar Energy **32** (1984) 211-222.

[8] C. M. Lampert, "*Heat mirror coatings for energy conserving windows"*, Solar Energy Materials **6** (1981) 1-41.

[9] C-C Lee, S-H Chen, and C-C. Jaing, "*Optical monitoring of silver-based transparent heat mirrors"*, Applied Optics **35** (1996) 5698-5703.

[10] P. H. Berning, "*Principles of design of architectural coatings*", Applied Optics **22** (1983) 4127-4141**.**

[11] **G**. Leftheriotis, P. Yianoulis and D. Patrikios, "*Deposition and optical properties of optimised ZnS/Ag/ZnS thin films for energy saving applications"*, Thin Solid Films **306** (1997) 92-99.

[12] B. E. Yoldas and T. O'Keefe, "*Deposition of optically transparent IR reflective coatings on glass"*, Applied Optics **23** (1984) 3638-3643.

[13] H. Kostlin and G. Frank, "*Optimization of transparent heat mirrors based on a thin silver film between antireflection films",* Thin Solid Films **89** (1982) 287-293.

[14] G. Leftheriotis, S. Papaefthimiou, P. Yanoulis, "*Integrated low emittance-electrochromic devices incorporating ZnS/Ag/ZnS coatings as transparent conductors*", Sol. Energy Mater. Sol. Cells **61** (2000) 107–112.

[15] J. C. Fan, F. J. Bachner, G. H. Foley, P. M. Zavracky, "*Transparent heat-mirror films of $TiO_2/Ag/TiO_2$ for solar energy collection and radiation insulation*", Appl. Phys. Lett. **25** (1974) 693.

[16] J. K. Fu, G. Atanassov, Y. S. Dai, F. H. Tan, Z. Q. Mo, "*Single films and heat mirrors produced by plasma ion assisted deposition*", J. Non-Crystalline Solids **218** (1997) 403-410.

[17] X. Zhang, S. Yu, M. Ma, *"ZnS/Me heat mirror systems"* Solar Energy Materials and Solar Cells **44** (1996) 279-290.

[18] D.R. Sahu, J.-L. Huang, "*High quality transparent conductive ZnO/Ag/ZnO multilayer films deposited at room temperature*", Thin Solid Films **515** (2006) 876–879.

[19] D.R. Sahu, J.-L. Huang, "*Characteristics of ZnO–Cu–ZnO multilayer films on copper layer properties*", Appl. Surf. Sci. **253** (2006) 827–832.

[20] J. George, B. Pradeep, and K. S. Joseph, "*Preparation of heat mirrors using Bismuth oxide films"*, phys. Stat. sol. (a) **100** (1987) 513-519.

[21] M. Okada, M. Tazawa, P. Jin, Y. Yamada, K. Yoshimura, "*Fabrication of photocatalytic heat-mirror with $TiO_2/TiN/TiO_2$ stacked layers"*, Vacuum **80** (2006) 732-735.

[22] Q.-N. Zhao, X.-J. Zhao, "*Preparation and characterization of $TiO_2/TiN/TiO_2$ multi-layer solar control coatings deposited by DC reactive magnetron sputtering at different substrate temperature*", J. Wuhan Univ. Technol. **16** (2001) 9–12.

[23] C-K. Jung, J-S. Moon, and J-H. Boo, "*High-rate and low-temperature synthesis of TiO_2, TiN, and TiO_2/Tin/TiO_2 thin films and study of their optical and interfacial characteristics"*, *J. Vac. Sci. Technol B* **23** (4) (2005) 1826-1831.

[24] K. E. Andersson, M. Veszelei, A. Roos, "*Zirconium nitride based transparent heat mirror coatings —preparation and characterization"*, Solar Energy Materials and Solar Cells **32** (1994) 199-212.

[25] R. E. Denton**,** R. D. Campbell, and S. G. Tomlin**,** *"The determination of optical constants of thin film coating materials"*, J**.** Phys**.** D **5** (1972) 852**–**863**.**

[26] S. M. A. Durrani, E. E. Khawaja, A. M. Al-Shukri, M. F. Al-Kuhaili, "*Dielectric/Ag/dielectric coated energy-efficient glass windows for warm climates"*, Energy and Building **36** (2004) 891-898.

[27] S. K. Deb and J. A. Chopoorian," *Optical Properties and Color-Center Formation in Thin Films of Molybdenum Trioxide*", J. Appl. Phys. **37** (1966) 4818.

[28] G. Leftheriotis, S. Papaefthimiou, P. Yianoulis, A. Siokou, "*Effect of the tungsten oxidation states in the thermal coloration and bleaching of amorphous WO_3 films*", Thin Solid Films **384**, (2001) 298-306.

[29] M. Tazawa, M. Okada, K. Yoshimura, S. Ikezawa*, "Photo-catalytic heat mirror with a thick titanium dioxide layer"*, Solar Energy Materials and Solar Cells **84** (2004) 159-170.

[30] K. Chiba and K. Nakatani, "*Photoenhance migration of silver atoms in transparent heat mirror coatings*", Thin Solid Films **112** (1984) 359-367.

[31] K. Chiba and K. Suzuki, "*Effects of heterogeneous metal atoms on the stability of a silver layer of a heat mirror coating*", Sol. Energy Mater. Sol. Cells **25** (1992) 113-123.

[32] Z. Wang, X. Cai, Q. Chen, P. K. Chu, "*Effects of Ti transition layer on stability of silver/titanium dioxide multilayered structure*", Thin Solids Films **515** (2007) 3146-3150.